The GTEx Consortium atlas of genetic regulatory effects across human tissues

GTEx Consortium

Published in:
Science (New York, N.Y.)

DOI:
10.1126/science.aaz1776

Publication date:
2020

Document Version
Peer reviewed version

The GTEx Consortium atlas of genetic regulatory effects across human tissues

The GTEx Consortium

Abstract

The Genotype-Tissue Expression (GTEx) project was established to characterize genetic effects on the transcriptome across human tissues, and to link these regulatory mechanisms to trait and disease associations. Here, we present analyses of the v8 data, examining 17,382 RNA-sequencing samples from 54 tissues of 948 post-mortem donors. We comprehensively characterize genetic associations for gene expression and splicing in *cis* and *trans*, showing that regulatory associations are found for almost all genes, and describe the underlying molecular mechanisms and their contribution to allelic heterogeneity and pleiotropy of complex traits. Leveraging the large diversity of tissues, we provide insights into the tissue-specificity of genetic effects and show that cell type composition is a key factor in understanding gene regulatory mechanisms in human tissues.

Introduction

A pressing need in human genetics remains the characterization and interpretation of the function of the millions of genetic variants across the human genome. This is essential for identifying the molecular mechanisms of genetic risk for complex traits and diseases, which are mainly driven by non-coding loci with largely uncharacterized regulatory functions. To address this challenge, several projects have built comprehensive annotations of genome function across tissues and cell types (*1*, *2*), and mapped the effects of regulatory variation across large numbers of individuals, primarily from whole blood and blood cell types (*3*-*5*). The Genotype-Tissue Expression (GTEx) project provides an essential intersection where variant function can be studied across a wide range of both tissues and individuals.

The GTEx project was launched in 2010 with the aim of building a catalog of genetic effects on gene expression across a large number of human tissues in order to elucidate the molecular mechanisms of genetic associations with complex diseases and traits, and improve our understanding of regulatory genetic variation (*6*). The project set out to collect biospecimens from ~50 tissues from up to ~1000 postmortem donors, and to create standards and protocols for optimizing postmortem tissue collection and donor recruitment (*7*, *8*), biospecimen processing (*7*), and data sharing (www.gtexportal.org).

Following the GTEx pilot (*9*) and mid-stage results (*10*), we present a final analysis of the v8 data release from the GTEx Consortium. We provide a catalog of genetic regulatory variants affecting gene expression and splicing in *cis* and *trans* across 49 tissues, and describe patterns and mechanisms of tissue- and cell type specificity of genetic regulatory effects. Through integration

of GTEx data with genome-wide association studies (GWAS), we characterize mechanisms of how genetic effects on the transcriptome mediate complex trait associations.

QTL discovery

The GTEx v8 data set consists of 948 donors and 17,382 samples from 52 tissues and two cell lines, with 838 donors and 15,253 samples having both RNA sequence (RNA-seq) and genotype data from whole genome sequencing (WGS) (Fig. 1A, and figs. S1 and S2). The 838 donors were 85.3% European American, 12.3% African American, and 1.4% Asian American. Of the 54 tissues, 49 had samples from at least 70 individuals and were used for analyses of quantitative trait loci (QTL) (15,201 samples total). WGS was performed for each donor to a median depth of 32x, resulting in the detection of a total of 43,066,422 single nucleotide variants (SNVs) after QC and phasing (10,008,325 with MAF $\geq$ 0.01) and 3,459,870 small indels (762,535 with MAF $\geq$ 0.01) (fig. S3 and table S1, (*11*)). The mRNA of each of the tissue samples was sequenced to a median depth of 82.6 million reads, and alignment, quantification and quality control were performed as described in (*11*) (figs. S4, S5, and S6).

The resulting data provide a broad survey of individual- and tissue- specific gene expression, enabling a comprehensive view of the impact of genetic variation on gene regulation (Fig. 1B). We mapped genetic loci that affect the expression (eQTL) or splicing (sQTL) of protein-coding and lincRNA genes, both in *cis* and *trans*. Genes with an eQTL or sQTL are called eGenes and sGenes, and significant variants eVariants and sVariants, respectively. Across all tissues, we discovered *cis*-eQTLs (5% FDR, per tissue (*11*) with 1% FDR results shown in fig. S7) for 18,262 protein coding and 5,006 lincRNA genes (23,268 total genes with a *cis*-eQTL, or *cis*-eGenes, corresponding to 94.7% of all protein coding and 67.3% of all detected lincRNA genes detected in at least one tissue), with a total of 4,278,636 genetic variants (43% of all variants with MAF $\geq$ 0.01) that were significant in at least one tissue (*cis*-eVariants) (Fig. 2A, figs. S7 and S8, and table S2). The discovered eQTLs had a high replication rate in external datasets (fig. S12 and S13). *Cis*-eQTLs for all long non-coding RNAs (lncRNAs), which include lincRNAs and other types, are characterized in a companion analysis (*12*). The genes lacking a *cis*-eQTL were enriched for those lacking expression in the tissues analyzed by GTEx, including genes involved in early development (fig. S9). While most of the discovered *cis*-eQTLs had small effect sizes measured as allelic fold change (aFC), across tissues an average of 22% of *cis*-eQTLs had an over 2-fold effect on gene expression (fig. S14). We mapped splicing QTLs (sQTLs) in *cis* with intron excision ratios from LeafCutter (*11*, *13*), and discovered 12,828 (66.5%) protein coding and 1,600 (21.5%) lincRNA genes (14,424 total) with a *cis*-sQTL (5% FDR, per tissue) in at least one tissue (*cis*-sVariants) (Fig. 2A, table S2, with 1% FDR results shown in fig. S7). As expected (*10*), *cis*-QTL discovery was highly correlated with the sample size for each tissue (Spearman's rho = 0.95 for *cis*-eQTLs, 0.92 for *cis*-sQTLs). The increased *cis*-eQTL discovery in larger tissues is primarily driven by additional power to discover small effects, with discovery of *cis*-eGenes with over two-fold effect saturating at ~1500 genes in tissues with >200 samples (fig. S14).

Previous studies have shown widespread allelic heterogeneity of gene expression in *cis,* i.e., multiple independent causal eQTLs per gene (*4*, *14*, *15*). We mapped independent *cis*-eQTLs and *cis*-sQTLs using stepwise regression, where the 5% FDR threshold for significance was defined by the single *cis*-QTL mapping (*10*). We observed widespread allelic heterogeneity, with up to 50% of eGenes having more than one independent *cis*-eQTL in the tissues with the largest sample sizes (Fig. 2B, and fig. S10). Our analysis captured a lower rate of allelic heterogeneity for *cis*-sQTLs, which can be a result of both underlying biology and lower power in *cis*-sQTL mapping (fig. S10). These results highlight gains in *cis*-eQTL mapping with increasing sample sizes even when the discovery of new eGenes in specific tissues starts to saturate.

Interchromosomal *trans*-eQTL mapping yielded 143 *trans*-eGenes (121 protein coding and 22 lincRNA at 5% FDR assessed at the gene level, separately for each gene type), after controlling for false positives due to read misalignment (*11*, *16*) (table S13). The number of *trans*-eGenes discovered per tissue is correlated with sample size (Spearman's rho = 0.68), and to the number of *cis*-eQTLs (rho = 0.77), with outlier tissues such as testis contributing disproportionately to both *cis* and *trans* (Fig. 2C). We identified a total of 49 *trans*-eGenes in testis, with 47 found in no other tissue even at FDR 50%. Over two-fold effect sizes on *trans*-eGene expression were observed for 19% of *trans*-eQTLs (fig. S14). *Trans*-sQTLs mapping yielded 29 *trans*-sGenes (5% FDR, per tissue), including a replication of a previously described *trans*-sQTL (*3*) and visual support of the association pattern in several loci (*11*) (fig. S11, table S14). These results suggest that while *trans*-sQTL mapping is challenging, we can discover robust genetic effects on splicing in *trans.*

We produced allelic expression (AE) data using two complementary approaches (*11*). In addition to the conventional AE data for each heterozygous genotype, we produced AE data by haplotype, integrating data from multiple heterozygous sites in the same gene, yielding 153 million gene-level measurements (≥8 reads) across all samples (*17*). Allelic expression reflects differential regulation of the two haplotypes in individuals that are heterozygous for a regulatory variant in *cis*; indeed, *cis*-eQTL effect size is strongly correlated with allelic expression (median rho = 0.82) (*10*). We hypothesized that *cis*-sQTLs could also partially contribute to allelic imbalance even if only for parts of transcripts. However, there is drastically less signal of increased allelic imbalance among individuals heterozygous for *cis*-sQTLs (median Spearman's rho = -0.05) (fig S15). This indicates that allelic expression data primarily captures *cis*-eQTL effects, and that genetic splicing variation in *cis* is not strongly reflected in gene-level AE data.

Genetic regulatory effects across populations and sexes

Variability in human traits and diseases between sexes and population groups is likely to partially derive from differences in genetic effects (*18-20*). To study whether genetic regulatory variants manifest this, we analyzed variable *cis*-eQTL effects between males and females, as well as between individuals of European and African ancestry. Since external replication data sets are sparse, we developed an allelic expression approach for validation with an orthogonal data type from the same samples (*17*): allelic imbalance in individuals heterozygous for the *cis*-eQTL allows individual-level quantification of the *cis*-eQTL effect size (*21*), and can be correlated with the

interaction terms used in *cis*-eQTL analysis to validate modifier effects of the *cis*-eQTL association (fig. S16).

To characterize sex-differentiated genetic effects on gene expression in GTEx tissues, we mapped sex-biased *cis*-eQTLs (sb-eQTLs). Analyzing the set of all conditionally independent *cis*-eQTLs, we identified eQTLs with significantly different effects between sexes by fitting a linear regression model and testing for a significant genotype-by-sex (G×S) interaction (*11*). Across the 44 GTEx tissues shared among sexes, we identified 369 sb-eQTLs (FDR ≤ 25%), characterized further in (*22*). Sex-biased eQTL discovery had a modest correlation with tissue sample size (Spearman's rho = 0.39, p = 0.03), with most sb-eQTLs discovered in breast but also in muscle, skin and adipose tissues. In some cases, the cis-eQTL signal — identified with males and females combined — seems to be driven exclusively by one sex. For example, the *cis*-eQTL association of rs2273535 with the gene *AURKA* in skeletal muscle (*cis*-eQTL $p = 6.92 \times 10^{24}$) is correlated with sex ($p_{G\times S} = 9.28 \times 10^{-12}$, Storey $q_{G\times S} = 1.07 \times 10^{-7}$, AE validation $p = 1.15 \times 10^{-11}$) and present only in males (Fig. 2D, and fig. S17). *AURKA* is a member of the serine/threonine kinase family involved in mitotic chromosomal segregation that has been widely studied as a risk factor in several cancers (*23*-*26*) and has been recently shown to be involved in muscle differentiation (*27*).

We also characterized population-biased *cis*-eQTLs (pb-eQTLs), where a variant's molecular effect on gene expression differs between individuals of European and African ancestry, controlling for differences in allele frequency, linkage disequilibrium (LD) and covariates (*11*). Analyzing 31 tissues with sample sizes >20 in both populations, we mapped genes with a different eQTL effect size measured by aFC. After applying stringent filters to remove differences potentially explained by LD or other artifacts (fig. S18A), we identified 178 pb-eQTLs for 141 eGenes (FDR ≤ 25%) that show a moderate degree of validation in allele-specific expression data (fig. S18C,D, table S10). While some of the pb-eQTL effects are tissue-specific, there are also effects that are shared across most tissues (fig. S18E). Fig. 2E shows an example of a pb-eQTL for the *SLC44A5* gene involved in transport of sugars and amino acids, and expressed at different levels between epidermis of lighter and darker skin (reconstructed *in vitro*) (*28*, *29*). In Europeans, the derived allele of rs4606268 decreases expression of the gene in esophagus mucosa (aFC = -4.82), but this effect is significantly lower in African Americans (aFC = -2.85, permutation p-value = 1.2×10^{-3}, AE validation p = 0.002, fig. S18C).

Altogether, despite the relaxed FDR, we discovered only a few hundred sex- or population-biased *cis*-eQTLs out of tens of thousands of *cis*-eQTLs in GTEx. This indicates that there are few regulatory variants with major modifier effects, and that these associations continue to be challenging to identify without a much larger sample size. However, the discovered effects can provide insights in to sex- or population-specific regulatory effects on gene expression. Importantly, factors correlated with sex or population, e.g., cell type composition or environmental exposures, may contribute to sex- or population-biased *cis*-eQTLs. These effects are described in detail in (*22*).

Fine-mapping

A major challenge of all genetic association studies is to distinguish the causal variants from their LD proxies. We applied three different statistical fine-mapping methods — CaVEMaN (*30*), CAVIAR (*31*), and dap-g (*32*) — to infer likely causal variants of *cis*-eQTLs in each tissue (Fig. 3A) (*11*). For many *cis*-eQTLs the causal variant can be mapped with a high probability to a handful of candidates: the 90% credible set for each *cis*-eQTL consists of variants that include the causal variant with 90% probability; using dap-g, we identified a median of 6 variants in the 90% credible set for each *cis*-eQTL (fig. S19). Furthermore, 9.3% of the *cis*-eQTLs have a variant with a posterior probability > 0.8 according to dap-g, indicating a single likely causal variant for those *cis*-eQTLs. We defined a consensus set of 24,740 *cis*-eQTLs across all tissues (7,709 unique variants), for which the posterior probability was >0.8 across all three methods (fig. S20). Fine-mapped variants were significantly more highly enriched among experimentally validated causal variants from MPRA (*33*) and SuRE (*34*), compared to the lead eVariant across all eGenes (Fig. 3B). The highest enrichment was observed for the consensus set although with overlapping confidence intervals (Fig. 3B). This demonstrates how careful fine-mapping facilitates the identification of likely causal regulatory variants.

Knowing the likely causal variant enables greater insights into the molecular mechanisms of individual eQTLs, including the mechanisms of their tissue-specific effects. Fig. 3C shows an example of an eQTL for the gene *CBX8* that colocalizes with breast cancer risk and birth weight (posterior probability 0.68 for both in lung). One of the three variants in the confident set overlaps the binding site and disrupts the motif of the transcription factor *EGR1* (*1*) (fig. S21). The role of *EGR1* as an upstream driver of this eQTL is further supported by a cross-tissue correlation of the effect size of the eQTL and the expression level of *EGR1* (Spearman's rho = -0.69) (Fig. 3D).

Functional mechanisms of QTL associations

Quantitative trait data from multiple molecular phenotypes, integrated with the regulatory annotation of the genome (table S3), offer a powerful way to understand the molecular mechanisms and phenotypic consequences of genetic regulatory effects. As expected, *cis*-eQTLs and *cis*-sQTLs are enriched in functional elements of the genome (Fig. 4A). While the strongest enrichments are driven by variant classes that lead to splicing changes or nonsense-mediated decay, these account for relatively few variants. *Cis*-sQTLs are enriched almost entirely in transcribed regions, while *cis*-eQTLs are enriched in transcriptional regulatory elements, as well. Previous studies (*4*, *35*) have indicated that *cis*-eQTL and *cis*-sQTL effects on the same gene are typically driven by different genetic variants. This is corroborated by the GTEx v8 data, where the overlap of *cis*-eQTL credible sets of likely causal variants, from CAVIAR analysis, have only a 12% overlap with *cis*-sQTL credible sets (fig. S22). Functional enrichment of overlapping and non-overlapping *cis*-eQTLs and *cis*-sQTLs, using stringent LD filtering, showed that the patterns characteristic for each type — such as enrichment of *cis*-eQTL in enhancers and *cis*-sQTLs in splice sites — are even stronger for distinct loci (fig. S22).

We hypothesized that eVariants and their target eGenes in *cis* are more likely to be in the same topologically associated domains (TADs) that allow chromatin interactions between more distant regulatory regions and target gene promoters (*36*). To test this, we analyzed TAD data from ENCODE (*1*) and *cis*-eQTLs from matching GTEx tissues (table S3). Compared to matching random variant-gene pairs and controlling for distance from the transcription start site, *cis*-eVariant-eGene pairs were significantly enriched for being in the same TAD (median OR 4.55; all $p<10^{-12}$) (fig. S23).

Trans-eQTLs are enriched in regulatory annotations that suggest both pre- and post-transcriptional mechanisms (Fig. 4B). Unlike *cis*-eQTLs, *trans*-eQTLs are enriched in CTCF binding sites, suggesting that disruption of CTCF binding may underlie distal genetic regulatory effects, potentially via its effect on interchromosomal chromatin interactions (*36*). *Trans*-eQTLs are also partially driven by *cis*-eQTLs (*37*, *38*). Indeed, we observed a significant enrichment of lead *trans*-eVariants tested in *cis* being also *cis*-eVariants in the same tissue (5.9x; two-sided Fisher's exact test $p = 5.03x10^{-22}$, Fig. 4C). A lack of analogous enrichment suggests that *cis*-sQTLs are less important contributors to *trans*-eQTLs ($p = 0.064$), and *trans*-sVariants had no significant enrichment of either *cis*-eQTLs ($p = 0.051$) or *cis*-sQTLs ($p = 0.53$). A further demonstration of the important contribution of *cis*-eQTLs to *trans*-eQTLs is that, on the basis of mediation analysis, 77% of lead *trans*-eVariants that are also *cis*-eVariants (corresponding to 31.6% of all lead *trans*-eVariants) appear to act through the *cis*-eQTL (Fig. 4D, and fig. S24). Colocalization of *cis*-eQTLs and *trans*-eQTLs was widespread and often tissue-specific, with Fig. 4E showing *cis*-eQTLs with at least ten nominally significant colocalized *trans*-eQTLs each (PP4 > 0.8 and *trans*-eQTL p-value < 10^{-5}), pinpointing how local effects on gene expression can potentially lead to downstream regulatory effects across the genome (fig. S25 and table S16). The many remaining *trans*-eQTLs that do coincide with a *cis*-eQTL may arise due to mechanisms including undetected *cis* effects in specific cell types or conditions, protein coding changes, effects on cell type heterogeneity, or more complex causality such as a variant that influences a trait with downstream consequences on gene expression.

Genetic regulatory effects mediate complex trait associations

In order to analyze the role of regulatory variants in genetic associations for human traits, we first asked whether variants in the GWAS catalog were enriched for significant QTLs, compared to all variants tested for QTLs (*11*). We observed a 1.46-fold enrichment for *cis*-eQTLs (63% vs 43%) and 1.86-fold enrichment for *cis*-sQTLs (37% vs 20%). The enrichment was even stronger, 6.97-fold (0.029% vs 0.0042%) for *trans*-eQTLs, consistent with other analyses (*39*) (Fig. 5A, fig. S26, tables S5 and S6). Cell type proportion may influence detection of *trans*-eQTLs in heterogeneous tissues, and may also be reflected in GWAS associations for blood cell count phenotypes and other complex traits. To minimize the possible impact of cell type heterogeneity on these enrichment statistics, we repeated these analyses among traits excluding blood cellularity traits. The resulting enrichments were 5.21-fold for *trans*-eQTLs, 1.43-fold for *cis*-eQTLs, and 1.81 for *cis*-sQTLs, largely preserving the patterns observed using the full set of GWAS traits.

This approach does not leverage the full power of genome-wide GWAS and QTL association statistics, nor account for LD contamination, a situation wherein the causal variants for QTL and GWAS signals are distinct but LD between the two causal variants can suggest a false functional link (*40*). Hence, for subsequent analyses (below) we selected 87 Genome Wide Association Studies (GWAS) representing a broad array of binary and continuous complex traits that have summary results available in the public domain (*11*, *41*), and *cis*-QTL statistics calculated from the European subset of GTEx donors to match the ancestry of GWAS studies (fig. S29). The analyses were performed for all pairwise combinations of 87 phenotypes and 49 tissues, and are summarized using an approach that accounts for similarity between tissues and variable standard errors of the QTL effect estimates, driven mainly by tissue sample size (fig. S27, and tables S4 and S11 (*11*)).

To analyze the mediating role of *cis*-regulation of gene expression on complex traits (*35*, *42*), we used two complementary approaches, QTLEnrich (*43*) and stratified LD score regression (S-LDSC) (*11*, *44*). To rule out the possibility that enrichment is driven by specific features of *cis*-QTLs such as allele frequency, distance to the transcription start site, or local level of LD (number of LD proxy variants; $r^2 \geq 0.5$), we used QTLEnrich. We found a 1.46-fold (SE=0.006) and 1.56-fold (SE=0.007) enrichment of trait associations among best *cis*-eQTLs and *cis*-sQTLs, respectively, adjusting for enrichment among matched null variants (Fig. 5A, table S7). The fact that these enrichment estimates differ little from those derived from the GWAS catalog overlap (above), even after accounting for the potential confounders, indicates how relatively robust these estimates are. Next, we used S-LDSC adjusting for functional annotations (*44*) to confirm the robustness of these results and to analyze how GWAS enrichment is affected by the causal e/sVariant being typically unknown (*11*). We computed the heritability enrichment of all *cis*-QTLs, fine-mapped *cis*-QTLs (in 95% credible set and posterior probability > 0.01 from dap-g), and fine-mapped *cis*-QTLs with maximum posterior inclusion probability as continuous annotation (MaxCPP) (*45*) (Fig. 5A). The largest increase in GWAS enrichment was for likely causal *cis*-QTL variants (11.1-fold (SE=1.2) for *cis*-eQTLs and 14.2-fold (SE=2.4) for and *cis*-sQTLs, for the continuous annotation), which is strong evidence of shared causal effects of *cis*-QTLs and GWAS, and for the importance of fine-mapping.

Joint enrichment analysis of *cis*-eQTLs and *cis*-sQTLs shows an independent contribution to complex trait variation from both (fig. S28, (*11*)), consistent with their limited overlap (fig. S22). The relative GWAS enrichments of *cis*-sQTLs and *cis*-eQTLs were similar (Fig. 5A; not significant for the robust QTLEnrich and LDSC analyses), but the larger number of *cis*-eQTLs discovered (Fig. 2) suggests a greater aggregated contribution of *cis*-eQTLs.

While these enrichment methods are powerful for genome-wide estimation of the QTL contribution to GWAS signals, they are not informative of regulatory mechanisms in individual loci. Thus, to provide functional interpretation of the 5,385 significant GWAS associations in 1,167 loci from approximately independent LD blocks (*46*) across the 87 complex traits, we performed colocalization with *enloc* (*32*) to quantify the probability that the *cis*-QTL and GWAS signals share the same causal variant. We also assessed the association between the genetically

regulated component of expression or splicing and complex traits with PrediXcan (*11*, *41*, *47*). Both methods take multiple independent *cis*-QTLs into account, which is critical in large *cis*-eQTL studies with widespread allelic heterogeneity, such as GTEx. Of the 5,385 GWAS loci, 43% and 23% were colocalized with a *cis*-eQTL and *cis*-sQTL, respectively (Fig. 5B). A large proportion of colocalized genes coincide with significant PrediXcan trait associations with predicted expression or splicing (median of 86% and 88% across phenotypes respectively; figs. S30, S31, S32, S33, tables S8, S15), with the full resource available in (*41*). While colocalization does not prove a causal role of a QTL in any given locus nor a genome-wide proportion of GWAS loci driven by eQTLs, these results suggest target genes and their potential molecular changes for thousands of GWAS loci, sometimes including both *cis* and *trans* targets (fig. S34).

Having multiple independent *cis*-eQTLs for a large number of genes allowed us to test whether mediated effects of primary and secondary *cis*-eQTLs on phenotypes — the ratio of GWAS and *cis*-eQTL effect sizes — are concordant. To make sure that concordance is not driven by residual LD between primary and secondary signals, we used LD-matched *cis*-eGenes with low colocalization probability as controls (*11*, *41*), and observed a significant increase in primary and secondary *cis*-eQTL concordance for colocalized genes (correlated t-test p-value $< 10^{-30}$; Fig. 5C). Additionally, colocalization of a *cis*-eQTL increased the colocalization of an independent *cis*-sQTL in the same locus (OR = 4.27, Fisher's exact test $p < 10^{-16}$), and correspondingly colocalization of a *cis*-sQTL increased *cis*-eQTL colocalization (OR = 4.54, Fisher's exact test $p < 10^{-16}$; figs. S35 and S36). This indicates that multiple regulatory effects for the same gene often mediate the same complex trait associations. Furthermore, genes with suggestive rare variant trait associations in the UK Biobank (*48*) have a substantially increased proportion of colocalized eQTLs for the same trait (Fig. 5D, and fig. S37), showing concordant trait effects from rare coding and common regulatory variants (*49*). These genes, as well as those with multiple colocalizing *cis*-QTLs, represent bona fide disease genes with multiple independent lines of evidence.

The growing number of genome and phenome studies has revealed extensive pleiotropy, where the same variant or locus associates with multiple organismal phenotypes (*50*). We sought to analyze how this phenomenon can be driven by gene regulatory effects. First, we calculated the number of *cis*-eGenes of each fine-mapped and LD-pruned *cis*-eVariant per tissue at local false sign rate (LFSR) < 5%, with cross-tissue smoothing of effect sizes with *mashr* (*11*, *51*). We observed that a median of 57% of variants were associated with more than one gene per tissue, typically co-occurring across tissues, indicating widespread regulatory pleiotropy. Using a binary classification of *cis*-eVariants with regulatory pleiotropy defined as those associated with more than one gene, we observed that they are more significantly associated with complex traits compared to matched *cis*-eVariants (fig. S38). This could be due to the fact that if a variant regulates multiple genes, there is a higher probability that at least one of them affects a GWAS phenotype. However, *cis*-eVariants with regulatory pleiotropy also have higher GWAS complex trait pleiotropy (*50*) than *cis*-eVariants with effects on a single gene (Fig. 5E). This observation suggests a mechanism for complex trait pleiotropy of genetic effects where the expression of multiple genes in *cis,* rather than a single eGene effect, translates into diverse downstream

physiological effects. Furthermore, GWAS pleiotropy is higher for tissue-shared (*41*) than tissue-specific *cis*-eQTLs, indicating that regulatory effects affecting multiple tissues are more likely to translate to diverse physiological traits (Fig. 5E).

Tissue-specificity of genetic regulatory effects

The GTEx data provide an opportunity to study patterns and mechanisms of tissue-specificity of the transcriptome and its genetic regulation. Pairwise similarity of GTEx tissues was quantified from gene expression and splicing, as well as allelic expression, eQTLs in *cis* and *trans*, and *cis*-sQTLs (Fig. 6A, and fig. S41, (*11*)). These estimates show consistent patterns of tissue relatedness, indicating that the biological processes that drive transcriptome similarity also control tissue sharing of genetic effects (Fig. 6B). As seen in earlier versions of the GTEx data (*9*, *10*), the brain regions form a separate cluster, and testis, LCLs, whole blood, and sometimes liver tend to be outliers, while most other organs have a notably high degree of similarity among each other. This indicates that blood is not an ideal proxy for most tissues, but that some other relatively accessible tissues, such as skin, may better capture molecular effects in other tissues.

The overall tissue specificity of QTLs ((*11*)) follows a U-shaped curve recapitulating previous GTEx analyses (*9*, *10*), where genetic regulatory effects tend to be either highly tissue-specific or highly shared (Fig. 6C), with *trans*-eQTLs being more tissue-specific than *cis*-eQTLs (fig. S40). *Cis*-sQTLs appear to be significantly more tissue specific than *cis*-eQTLs when considering all mapped *cis*-QTLs, but this pattern is reversed when considering only those *cis*-QTLs where the gene or splicing event is quantified in all tissues (Fig. 6C, and fig. S39). This indicates that splicing measures are more tissue-specific than gene expression, but genetic effects on splicing tend to be more shared, consistent with pairwise tissue sharing patterns (fig. S41). This is important for understanding effects that disease-causing splicing variants may have across tissues, and for validation of splicing effects in cell lines that rarely are an exact match to cells *in vivo*. Next, we analyzed the sharing of allelic expression (AE) across multiple tissues of an individual, which is a metric of sharing of any heterozygous regulatory variant effects in that individual. Variation in AE has been useful for analysis of rare, potentially disease-causing variants (*52*). Using a clustering approach (*11*), we found that in 97.4% of the cases, AE across all tissues forms a single cluster. This suggests that in AE analysis, different tissues are often relatively good proxies for one another, provided that the gene of interest is expressed in the probed tissue. (fig. S42).

We next computed the cross-tissue correlation of eQTL effect size and eGene expression level — often a proxy for gene functionality — and discovered that 1,971 *cis*-eQTLs (7.4%; FDR 5%) had a significant and robust correlation between eGene expression and *cis*-eQTL effect size across tissues (Fig 6D, and fig. S43). These correlated *cis*-eQTLs are split nearly evenly between negative (937) and positive (1,034) correlations. Thus, the tissues with the highest *cis*-eQTL effect sizes are equally likely to be among tissues with higher or lower expression levels for the gene.

Trans-eQTLs show a different pattern, being typically observed in tissues with high expression of the *trans*-eGene relative to other tissues (fig. S43).

These observations raise the question of how to prioritize the relevant tissues for eQTLs in a disease context. To address this, we chose a subset of GWAS traits with a strong prior indication for the likely relevant tissue(s) (table S12). Analyzing colocalized *cis*-eQTLs for 1,778 GWAS loci (*11*), we discovered that the relevant tissues were significantly enriched in having high expression and effect sizes (paired Wilcoxon sign test $p<1.5e^{-4}$), but the relatively weak signal indicates that pinpointing the likely relevant tissue GWAS loci is challenging (figs. S44, S45, table S9). This indicates that both effect sizes and gene expression levels are important for interpreting the tissue context where an eQTL may have downstream phenotypic effects.

The diverse patterns of QTL tissue-specificity raise the question of what molecular mechanisms underlie the ubiquitous regulatory effects of some genetic variants and the highly tissue-specific effects of others. To gain insight into this question, we modeled *cis*-eQTL and *cis*-sQTL tissue specificity using logistic regression as a function of the lead eVariant's genomic and epigenomic context (*11*). *Cis*-QTLs where the top eVariant was in a transcribed region had overall higher sharing than those in classical transcriptional regulatory elements, indicating that genetic variants with post- or co-transcriptional expression or splicing effects have more ubiquitous effects (Fig. 6E). Canonical splice and stop gained variant effects had the highest probability of being shared across tissues, which may benefit disease-focused studies relying on likely gene-disrupting variants. We also considered whether varying regulatory activity between tissues contributed to tissue-specificity of genetic effects, and found that shared chromatin states between the discovery and query tissues were associated with increased probability of *cis*-eQTL sharing and vice-versa (Fig. 6F). *cis*-eQTLs and *cis*-sQTLs followed similar patterns. Since *cis*-sQTLs are more enriched in transcribed regions and likely arise via post-transcriptional mechanisms (Fig. 4A), this is likely to contribute to their higher overall degree of tissue-sharing (Fig. 6C). In comparison to *cis*-eQTLs, *cis*-sQTLs are more often located in regions where regulatory effects are shared.

These data indicate a possible means by which we can predict if a *cis*-eQTL observed in a GTEx tissue is active in another tissue of interest, using the variant's annotation and properties in the discovery tissue (*11*). After incorporating additional features including *cis*-QTL effect size, distance to transcription start site, and eGene/sGene expression levels, we obtain reasonably good predictions of whether a *cis*-QTL is active in a query tissue (median AUC = 0.779 and 0.807, min = 0.703 and 0.721, max = 0.807 and 0.875 for *cis*-eQTLs and *cis*-sQTLs, respectively; fig. S46). This suggests that it is possible to extrapolate the GTEx *cis*-eQTL catalog to additional tissues and potentially developmental stages, where population-scale data for QTL analysis are particularly difficult to collect.

From tissues to cell types

The GTEx tissue samples consist of heterogeneous mixtures of multiple cell types. Hence, the RNA extracted and QTLs mapped from these samples reflect a composite of genetic effects that may vary across cell types and may mask cell type-specific mechanisms. To characterize the

effect of cell type heterogeneity on analyses from bulk tissue, we used the xCell method (*53*) to estimate the enrichment of 64 reference cell types from the bulk expression profile of each sample (*11*). While these results need to be interpreted with caution given the scarcity of validation data (*54*), the resulting enrichment scores were generally biologically meaningful with, for example, myocytes enriched in heart left ventricle and skeletal muscle, hepatocytes enriched in liver, and various blood cell types enriched in whole blood, spleen, and lung, which harbors a large leukocyte population (fig. S47). Interestingly, the pairwise relatedness of GTEx tissues derived from their cell type composition is highly correlated with tissue-sharing of regulatory variants (*cis*-eQTL versus cell type composition Rand index = 0.92; Fig. 6B, and figs. S48 and S41), suggesting that similarity of regulatory variant activity between tissue pairs may often be due to the presence of similar cell types, and not necessarily shared regulatory networks within cells. This highlights the key role that characterizing cell type diversity will have for understanding not only tissue biology but genetic regulatory effects as well.

Enrichment of many cell types shows inter-individual variation within a given tissue, partially due to tissue sampling variation between individuals. This variation can be leveraged to identify *cis*-eQTLs and *cis*-sQTLs with cell type specificity, by including an interaction between genotype and cell type enrichment in the QTL model (*11*, *55*). We applied this approach to seven tissue-cell type pairs with robustly quantified cell types in the tissue where each cell type was most enriched (Fig. 7A; an additional 36 pairs are described in (*54*)). The largest numbers of cell type interacting *cis*-eQTLs and *cis*-sQTLs (ieQTLs and isQTLs) were 1120 neutrophil ieQTLs and 169 isQTLs in whole blood and 1087 epithelial cell ieQTLs and 117 isQTLs in transverse colon (Fig. 7A). Of these ieQTLs, 76 and 229, respectively, involved an eGene for which no QTL was detected in bulk tissue. We validated these effects using published eQTLs from purified blood cell types (*56*), where neutrophil eQTLs had higher neutrophil ieQTL effect sizes than eQTLs from other blood cell types (fig. S49). For other cell types, external replication data was not available. Thus, we verified the robustness of the ieQTLs by the allelic expression validation approach that was used for sex- and population-biased *cis*-eQTL analyses: for ieQTL heterozygotes, we calculated the Spearman correlation between cell type enrichment and ieQTL effect size from AE data, and observed a high validation rate (*54*). It is important to note that ie/isQTLs should not be considered cell type-specific QTLs, because the enrichment of any cell type may be (anti-)correlated with other cell types (fig. S50). While full deconvolution of *cis*-eQTL effects driven by specific cell types remains a challenge for the future, ieQTLs and isQTLs can be interpreted as being enriched for cell type-specific effects.

In most subsequent analyses to characterize the properties of ieQTLs and isQTLs, we focused on neutrophil ieQTLs, which are numerous and supported by external replication data. Functional enrichment analyses of these QTLs show that these largely follow the enrichment patterns observed for bulk tissue *cis*-QTLs (Fig. 7B). However, ieQTLs are more strongly enriched in promoter flanking regions and enhancers, which are known to be major drivers of cell type specific regulatory effects (*2*). Epithelial cell ieQTLs yielded similar patterns (fig. S51).

We hypothesized that the widespread allelic heterogeneity observed in the bulk tissue *cis*-eQTL data could be partially driven by an aggregate signal from *cis*-eQTLs that are each active in a different cell type present in the tissue. Indeed, the number of *cis*-eQTLs per gene is higher for ieGenes than for standard eGenes, especially in skin and blood (Fig. 7C). While differences in power could contribute to this pattern, it is corroborated by eGenes that have independent *cis*-eQTLs ($r^2 < 0.05$) in five purified blood cell types (*56*) also showing an increased amount of allelic heterogeneity in GTEx whole blood (Fig. 7C and D). Thus, quantifying cell type specificity can provide mechanistic insights into the genetic architecture of gene expression, and may be leveraged to improve the resolution of complex patterns of allelic heterogeneity where we can distinguish effects manifesting in different cell types.

Next, we analyzed how cell type interacting *cis*-QTLs contribute to the interpretation of regulatory variants underlying complex disease risk. GWAS colocalization analysis of neutrophil ieQTLs (*11*) revealed multiple loci (111, ~32%) that colocalize only with ieQTLs and not with whole blood *cis*-eQTLs (Fig. 7E), even though 75% (42/56) of the corresponding eGenes have both *cis*-eQTLs and ieQTLs. Improved resolution into allelic heterogeneity appears to contribute to this. For example, the absence of colocalization between a platelet count GWAS signal and bulk tissue *cis*-eQTL for *SPAG7* appears to be due to the whole blood signal being an aggregate of multiple independent signals (fig. S52). The neutrophil ieQTL analysis uncovers a specific signal that mirrors the GWAS association, suggesting that platelet counts are affected by *SPAG7* expression only in specific cell type(s). Thus, in addition to previously undetected colocalizations pinpointing potential causal genes, ieQTL analysis has the potential to provide insights into cell type specific mechanisms of complex traits.

Discussion

The GTEx v8 data release represents a deep survey of both intra- and inter-individual transcriptome variation across a large number of tissues. With 838 donors and 15,253 samples — approximately twice the size of the v6 release used in the previous set of GTEx Consortium papers — we have created a comprehensive resource of genetic variants that influence gene expression and splicing in *cis*. This significantly expands and updates the GTEx catalog of sQTLs, doubles the number of eGenes per tissue, and saturates the discovery of eQTLs with over 2-fold effect sizes in ~40 tissues. The fine-mapping data of GTEx *cis*-eQTLs provides a set of thousands of likely causal functional variants. While *trans*-QTL discovery, as well as characterization of sex-specific and population-specific genetic effects, are still limited by sample size, analyses of the v8 data provide important insights into each. Cell type interacting *cis*-eQTLs and *cis*-sQTLs, mapped with computational estimates of cell type enrichment, constitute an important extension of the GTEx resource to effects of cell types within tissues. The strikingly similar tissue-sharing patterns across these data types suggests shared biology from cell type composition to transcriptome variation and genetic regulatory effects. Our results indicate that shared cell types between tissues may be a key factor behind tissue-sharing of genetic regulatory effects, which will constitute a key challenge to

tackle in the future. Finally, GWAS colocalization with *cis*-eQTLs and *cis*-sQTLs provides rich opportunities for further functional follow-up and characterization of regulatory mechanisms of GWAS associations.

Given the very large number of *cis*-eQTLs, the extensive allelic heterogeneity – multiple independent regulatory variants affecting the same gene – is unsurprising. With well-powered *cis*-QTL mapping, it becomes possible and important to describe and disentangle these effects; the assumption of a single causal variant in a *cis*-eQTL locus no longer holds true for data sets of this scale. Similarly, we highlight *cis*-eQTL and *cis*-sQTL effects on the same gene, typically driven by distinct causal variants (*4*, *35*). The joint complex trait contribution of independent *cis*-eQTLs and *cis*-sQTLs, and *cis*-eQTLs and rare coding variants for the same gene highlights how different genetic variants and functional perturbations can converge at the gene level to similar physiological effects. This orthogonal evidence pinpoints highly likely causal disease genes, and these associations could be leveraged to build allelic series, a powerful tool for estimating dosage-risk relationship for the purposes of drug development (*57*). Finally, we provide mechanistic insights into the cellular causes of allelic heterogeneity, showing the separate contributions from *cis*-eQTLs active in different cell types to the combined signal seen in a bulk tissue sample. With evidence that this increased cellular resolution improves colocalization in some loci, cell type specific analyses appear particularly promising for finer dissection of genetic association data.

Integration of GTEx QTL data and functional annotation of the genome provides powerful insights into the molecular mechanisms of transcriptional and post-transcriptional regulation that affect gene expression levels and splicing. A large proportion of *cis*-eQTL effects are driven by genetic perturbations in classical regulatory elements of promoters and enhancers. However, the magnitude of these enrichments is perhaps surprisingly modest, which likely reflects the fact that only a small fraction of variants in these large regions have true regulatory effects, leading to a lower resolution of annotating functional variants compared to the nucleotide-level annotation of, e.g., nonsense or canonical splice site variants. Context-specific genetic effects of tissue-specific and cell-type interacting *cis*-eQTLs are enriched in enhancers and related elements and their variable activity across tissues and cell types. While *cis*-eQTLs are enriched for a wide range of functional regions, the vast majority of *cis*-sQTL are located in transcribed regions, with likely co-/post-transcriptional regulatory effects. Interestingly, these appear to be less tissue-specific, which likely contributes to the higher tissue-sharing of *cis*-sQTLs than *cis*-eQTLs. The higher tissue-sharing of all co/post-transcriptional regulatory effects may facilitate interpretation of potentially disease-related functional effects of (rare) coding variants triggering nonsense-mediated decay or splicing changes, even when the disease-relevant tissues are not available.

Approximately a third of the observed *trans*-eQTLs are mediated by *cis*-eQTLs, demonstrating how local genetic regulatory effects can translate to effects at the level of cellular pathways. All types of QTLs that were studied are strong mediators of genetic associations to complex traits, with a higher relative enrichment for *cis*-sQTLs than *cis*-eQTLs, with *trans*-eQTLs having the

highest enrichment of all (*35*). With large genome- and phenome-wide (GWAS/PheWAS) studies having uncovered extensive pleiotropy of complex trait associations, the GTEx data provide important insights into the molecular underpinnings of this observed pleiotropy: variants that affect the expression of multiple genes and multiple tissues have a higher degree of complex trait pleiotropy, indicating that some of the pleiotropy arises at the proximal regulatory level. Dissecting this complexity and pinpointing truly causal molecular effects that mediate specific phenotype associations will be a considerable challenge for the future.

This study of the GTEx v8 data has provided insights into genetic regulatory architecture and functional mechanisms. The catalog of QTLs and associated data sets of annotations, cell type enrichments, and GWAS summary statistics requires careful interpretation but provides insights into the biology of gene regulation and functional mechanisms of complex traits. We demonstrate how QTL data can be used to inform on multiple layers of GWAS interpretation: potential causal variants from fine-mapping, proximal regulatory mechanisms, target genes in *cis*, pathway effects in *trans*, in the context of multiple tissues and cell types. However, our understanding of genetic effects on cellular phenotypes is far from complete. We envision that further investigation into genetic regulatory effects in specific cell types, study of additional tissues and developmental time points not covered by GTEx, incorporation of a diverse set of molecular phenotypes, and continued investment in increasing sample sizes from diverse populations will continue to provide transformative scientific discoveries.

References

[1] ENCODE Project Consortium, An integrated encyclopedia of DNA elements in the human genome. Nature 489, 57–74 (2012).

[2] Roadmap Epigenomics Consortium, et al., Integrative analysis of 111 reference human epigenomes. Nature 518, 317–330 (2015).

[3] A. Battle, et al., Characterizing the genetic basis of transcriptome diversity through RNA-sequencing of 922 individuals. Genome Research 24, 14–24 (2014).

[4] T. Lappalainen, et al., Transcriptome and genome sequencing uncovers functional variation in humans. Nature 501, 506–511 (2013).

[5] M. J. Bonder, et al., Disease variants alter transcription factor levels and methylation of their binding sites. Nature Genetics 49, 131–138 (2017).

[6] GTEx Consortium, The Genotype-Tissue Expression (GTEx) project. Nature Genetics 45, 580–585 (2013).

[7] L. J. Carithers, et al., A Novel Approach to High-Quality Postmortem Tissue Procurement: The GTEx Project. Biopreservation and biobanking 13, 311–319 (2015).

[8] L. A. Siminoff, M. Wilson-Genderson, H. M. Gardiner, M. Mosavel, K. L. Barker, Consent to a Postmortem Tissue Procurement Study: Distinguishing Family Decision Makers' Knowledge of the Genotype-Tissue Expression Project. Biopreservation and biobanking 16, 200–206 (2018).

[9] GTEx Consortium, The Genotype-Tissue Expression (GTEx) pilot analysis: multitissue gene regulation in humans. Science 348, 648–660 (2015).

[10] GTEx Consortium, Genetic effects on gene expression across human tissues. Nature 550, 204–213 (2017).

[11] See supplementary materials.

[12] O. M. de Goede, et al., Long non-coding RNA gene regulation and trait associations across human tissues. bioRxiv (2019).

[13] Y. I. Li, et al., Annotation-free quantification of RNA splicing using LeafCutter. Nature Genetics 50, 151–158 (2018).

[14] R. Jansen, et al., Conditional eQTL analysis reveals allelic heterogeneity of gene expression. Human molecular genetics 26, 1444–1451 (2017).

[15] F. Hormozdiari, et al., Widespread Allelic Heterogeneity in Complex Traits. American Journal of Human Genetics 100, 789– 802 (2017).

[16] A. Saha, A. Battle, False positives in trans-eQTL and co-expression analyses arising from RNA-sequencing alignment errors. F1000Research 7, 1860–27 (2018).

[17] S. E. Castel, F. Aguet, P. Mohammadi, K. G. Ardlie, T. Lappalainen, A vast resource of allelic expression data spanning human tissues. bioRxiv (2019).

[18] E. A. Khramtsova, L. K. Davis, B. E. Stranger, The role of sex in the genomics of human complex traits. Nature Reviews Genetics 20, 173–190 (2019).

[19] B. E. Stranger, et al., Patterns of cis regulatory variation in diverse human populations. PLoS Genetics 8, e1002639 (2012).

[20] T. Raj, et al., Polarization of the effects of autoimmune and neurodegenerative risk alleles in leukocytes. Science 344, 519–523 (2014).

[21] P. Mohammadi, S. E. Castel, A. A. Brown, T. Lappalainen, Quantifying the regulatory effect size of cis-acting genetic variation using allelic fold change. Genome Research 27, 1872–1884 (2017).

[22] M. Oliva, et al., The role of sex in the human transcriptome. bioRxiv (2019).

[23] T. Sun, et al., Functional Phe31Ile polymorphism in Aurora A and risk of breast carcinoma. Carcinogenesis 25, 2225–2230 (2004).

[24] A. Ewart-Toland, et al., Aurora-A/STK15 T+91A is a general low penetrance cancer susceptibility gene: a meta-analysis of multiple cancer types. Carcinogenesis 26, 1368–1373 (2005).

[25] Y. Ruan, et al., Genetic polymorphisms in AURKA and BRCA1 are associated with breast cancer susceptibility in a Chinese Han population. The Journal of Pathology 225, 535–543 (2011).

[26] H. M. Koh, et al., Aurora Kinase A Is a Prognostic Marker in Colorectal Adenocarcinoma. Journal of pathology and translational medicine 51, 32–39 (2017).

[27] K. Dhanasekaran, et al., Unraveling the role of aurora A beyond centrosomes and spindle assembly: implications in muscle differentiation. The FASEB Journal 33, 219–230 (2019).

[28] S. Girardeau-Hubert, et al., Reconstructed Skin Models Revealed Unexpected Differences in Epidermal African and Caucasian Skin. Scientific Reports 9, 7456 (2019).

[29] L. Yin, et al., Epidermal gene expression and ethnic pigmentation variations among individuals of Asian, European and African ancestry. Experimental dermatology 23, 731–735 (2014).

[30] A. A. Brown, et al., Predicting causal variants affecting expression by using whole-genome sequencing and RNA-seq from multiple human tissues. Nature Genetics 49, 1747–1751 (2017).

[31] F. Hormozdiari, E. Kostem, E. Y. Kang, B. Pasaniuc, E. Eskin, Identifying causal variants at loci with multiple signals of association. Genetics 198, 497–508 (2014).

[32] X. Wen, R. Pique-Regi, F. Luca, Integrating molecular QTL data into genome-wide genetic association analysis: Probabilistic assessment of enrichment and colocalization. PLoS Genetics 13, e1006646 (2017).

[33] R. Tewhey, et al., Direct Identification of Hundreds of Expression-Modulating Variants using a Multiplexed Reporter Assay. Cell 165, 1519–1529 (2016).

[34] J. van Arensbergen, et al., Systematic identification of human SNPs affecting regulatory element activity. bioRxiv (2019).

[35] Y. I. Li, et al., RNA splicing is a primary link between genetic variation and disease. Science 352, 600–604 (2016).

[36] O. Delaneau, et al., Chromatin three-dimensional interactions mediate genetic effects on gene expression. Science 364 (2019).

[37] K. S. Small, et al., Identification of an imprinted master trans regulator at the KLF14 locus related to multiple metabolic phenotypes. Nature Genetics 43, 561–564 (2011).

[38] F. Yang, J. Wang, GTEx Consortium, B. L. Pierce, L. S. Chen, Identifying cis-mediators for trans-eQTLs across many human tissues using genomic mediation analysis. Genome Research 27, 1859–1871 (2017).

[39] H.-J. Westra, et al., Systematic identification of trans eQTLs as putative drivers of known disease associations. Nature Genetics 45, 1238–1243 (2013).

[40] B. Liu, M. J. Gloudemans, A. S. Rao, E. Ingelsson, S. B. Montgomery, Abundant associations with gene expression complicate GWAS follow-up. Nature Genetics 51, 768–769 (2019).

[41] A. N. Barbeira, et al., Exploiting the GTEx resources to decipher the mechanisms at GWAS loci. bioRxiv 42, 814350 (2020).

[42] D. L. Nicolae, et al., Trait-associated SNPs are more likely to be eQTLs: annotation to enhance discovery from GWAS. PLoS Genetics 6, e1000888 (2010).
[43] E. R. Gamazon, et al., Using an atlas of gene regulation across 44 human tissues to inform complex disease- and trait-associated variation. Nature Genetics 50, 956–967 (2018).

[44] H. K. Finucane, et al., Partitioning heritability by functional annotation using genome-wide association summary statistics. Nature Genetics 47, 1228–1235 (2015).

[45] F. Hormozdiari, et al., Leveraging molecular quantitative trait loci to understand the genetic architecture of diseases and complex traits. Nature Genetics 50, 1041–1047 (2018).

[46] T. Berisa, J. K. Pickrell, Approximately independent linkage disequilibrium blocks in human populations. Bioinformatics 32, 283–285 (2016).

[47] E. R. Gamazon, et al., A gene-based association method for mapping traits using reference transcriptome data. Nature Genetics 47, 1091–1098 (2015).

[48] E. T. Cirulli, et al., Genome-wide rare variant analysis for thousands of phenotypes in 54,000 exomes. bioRxiv 442, 199–22 (2019).

[49] N. M. Ferraro, et al., Diverse transcriptomic signatures across human tissues identify functional rare genetic variation. bioRxiv (2019).

[50] D. M. Jordan, M. Verbanck, R. Do, HOPS: a quantitative score reveals pervasive horizontal pleiotropy in human genetic variation is driven by extreme polygenicity of human traits and diseases. Genome Biology 20, 222–18 (2019).

[51] S. M. Urbut, G. Wang, P. Carbonetto, M. Stephens, Flexible statistical methods for estimating and testing effects in genomic studies with multiple conditions. Nature Genetics 51, 187–195 (2019).

[52] P. Mohammadi, et al., Genetic regulatory variation in populations informs transcriptome analysis in rare disease. Science 366, 351–356 (2019).

[53] D. Aran, Z. Hu, A. J. Butte, xCell: digitally portraying the tissue cellular heterogeneity landscape. Genome Biology 18, 220 (2017).

[54] S. Kim-Hellmuth, et al., Cell type specific genetic regulation of gene expression across human tissues. bioRxiv 7, 1860 (2019).

[55] D. V. Zhernakova, et al., Identification of context-dependent expression quantitative trait loci in whole blood. Nature Genetics 49, 139–145 (2017).

[56] J. E. Peters, et al., Insight into Genotype-Phenotype Associations through eQTL Mapping in Multiple Cell Types in Health and Immune-Mediated Disease. PLoS Genetics 12, e1005908 (2016).

[57] R. M. Plenge, E. M. Scolnick, D. Altshuler, Validating therapeutic targets through human genetics. Nature 12, 581–594 (2013).

[58] S. Fisher, et al., A scalable, fully automated process for construction of sequence-ready human exome targeted capture libraries. Genome Biology 12, R1 (2011).

[59] T. Tukiainen, et al., Landscape of X chromosome inactivation across human tissues. Nature 550, 244–248 (2017).

[60] D. Kim, B. Langmead, S. L. Salzberg, HISAT: a fast spliced aligner with low memory requirements. Nature Methods 12, 357–360 (2015).

[61] R. E. Handsaker, et al., Large multiallelic copy number variations in humans. Nature Genetics 47, 296–303 (2015).

[62] O. Delaneau, J.-F. Zagury, J. Marchini, Improved whole-chromosome phasing for disease and population genetic studies. Nature Methods 10, 5–6 (2013).

[63] A. Dobin, et al., STAR: ultrafast universal RNA-seq aligner. Bioinformatics 29, 15–21 (2013).

[64] B. van de Geijn, G. McVicker, Y. Gilad, J. K. Pritchard, WASP: allele-specific software for robust molecular quantitative trait locus discovery. Nature Methods 12, 1061–1063 (2015).

[65] F. A. Wright, et al., Heritability and genomics of gene expression in peripheral blood. Nature Genetics 46, 430–437 (2014).

[66] D. S. DeLuca, et al., RNA-SeQC: RNA-seq metrics for quality control and process optimization. Bioinformatics 28, 1530– 1532 (2012).

[67] M. D. Robinson, A. Oshlack, A scaling normalization method for differential expression analysis of RNA-seq data. Genome Biology 11, R25 (2010).

[68] O. Stegle, L. Parts, R. Durbin, J. Winn, A Bayesian framework to account for complex non-genetic factors in gene expression levels greatly increases power in eQTL studies. PLoS Computational Biology 6, e1000770 (2010).

[69] N. R. Gay, et al., Impact of admixture and ancestry on eQTL analysis and GWAS colocalization in GTEx. bioRxiv 95, 1.22.1 (2019).

[70] H. Ongen, A. Buil, A. A. Brown, E. T. Dermitzakis, O. Delaneau, Fast and efficient QTL mapper for thousands of molecular phenotypes. Bioinformatics 32, 1479–1485 (2016).

[71] J. D. Storey, R. Tibshirani, Statistical significance for genomewide studies. PNAS 100, 9440–9445 (2003).

[72] A. Taylor-Weiner, et al., Scaling computational genomics to millions of individuals with GPUs. Genome Biology 20, 228–5 (2019).

[73] C. Giambartolomei, et al., Bayesian test for colocalisation between pairs of genetic association studies using summary statistics. PLoS Genetics 10, e1004383 (2014).

[74] A. Buil, et al., Gene-gene and gene-environment interactions detected by transcriptome sequence analysis in twins. Nature Genetics 47, 88–91 (2015).

[75] U. Võsa, et al., Unraveling the polygenic architecture of complex traits using blood eQTL metaanalysis. bioRxiv 100, 228 (2018).

[76] S. E. Castel, A. Levy-Moonshine, P. Mohammadi, E. Banks, T. Lappalainen, Tools and best practices for data processing in allelic expression analysis. Genome Biology 16, 195 (2015).

[77] N. I. Panousis, M. Gutierrez-Arcelus, E. T. Dermitzakis, T. Lappalainen, Allelic mapping bias in RNA-sequencing is not a major confounder in eQTL studies. Genome Biology 15, 467 (2014).

[78] S. E. Castel, P. Mohammadi, W. K. Chung, Y. Shen, T. Lappalainen, Rare variant phasing and haplotypic expression from RNA sequencing with phASER. Nature Communications 7, 12817 (2016).

[79] S. Anders, W. Huber, Differential expression analysis for sequence count data. Genome Biology 11, R106–12 (2010).

[80] D. R. Zerbino, S. P. Wilder, N. Johnson, T. Juettemann, P. R. Flicek, The ensembl regulatory build. Genome Biology 16, 56 (2015).

[81] X. Wen, Molecular QTL discovery incorporating genomic annotations using Bayesian false discovery rate control. The Annals of Applied Statistics 10, 1619–1638 (2016).

[82] K. Michailidou, et al., Association analysis identifies 65 new breast cancer risk loci. Nature 551, 92–94 (2017).

[83] B. Tang, et al., CBX8 exhibits oncogenic properties and serves as a prognostic factor in hepatocellular carcinoma. Cell death & disease 10, 52–14 (2019).

[84] C.-Y. Chung, et al., Cbx8 Acts Non-canonically with Wdr5 to Promote Mammary Tumorigenesis. Cell Reports 16, 472–486 (2016).

[85] C. Z. Zhang, et al., CBX8 Exhibits Oncogenic Activity via AKT/β-Catenin Activation in Hepatocellular Carcinoma. Cancer Research 78, 51–63 (2018).

[86] A. Buniello, et al., The NHGRI-EBI GWAS Catalog of published genome-wide association studies, targeted arrays and summary statistics 2019. Nucleic Acids Research 47, D1005–D1012 (2019).

[87] D. Lee, T. B. Bigdeli, B. P. Riley, A. H. Fanous, S.-A. Bacanu, DIST: direct imputation of summary statistics for unmeasured SNPs. Bioinformatics 29, 2925–2927 (2013).

[88] B. Pasaniuc, et al., Fast and accurate imputation of summary statistics enhances evidence of functional enrichment. Bioinformatics 30, 2906–2914 (2014).

[89] X. Wen, Y. Lee, F. Luca, R. Pique-Regi, Efficient Integrative Multi-SNP Association Analysis via Deterministic Approximation of Posteriors. American Journal of Human Genetics 98, 1114–1129 (2016).

[90] S. Gazal, et al., Linkage disequilibrium-dependent architecture of human complex traits shows action of negative selection. Nature Genetics 49, 1421–1427 (2017).

[91] A. N. Barbeira, et al., Exploring the phenotypic consequences of tissue specific gene expression variation inferred from GWAS summary statistics. Nature Communications 9, 1825–20 (2018).

[92] A. N. Barbeira, et al., Integrating predicted transcriptome from multiple tissues improves association detection. PLoS Genetics 15, e1007889 (2019).

[93] J. Friedman, T. Hastie, R. Tibshirani, Regularization Paths for Generalized Linear Models via Coordinate Descent. Journal of statistical software 33, 1–22 (2010).

[94] International HapMap 3 Consortium, et al., Integrating common and rare genetic variation in diverse human populations. Nature 467, 52–58 (2010).

[95] C. Wang, et al., Deletion of mstna and mstnb impairs the immune system and affects growth performance in zebrafish. Fish & shellfish immunology 72, 572–580 (2018).

[96] Y. Y. Wan, GATA3: a master of many trades in immune regulation. Trends in immunology 35, 233–242 (2014).

[97] W. Wang, M. Stephens, Empirical Bayes Matrix Factorization. arXiv.org (2018).

[98] J. H. Sul, B. Han, C. Ye, T. Choi, E. Eskin, Effectively identifying eQTLs from multiple tissues by combining mixed model and meta-analytic approaches. PLoS Genetics 9, e1003491 (2013).

[99] X. Zhou, M. Stephens, Genome-wide efficient mixed-model analysis for association studies. Nature Genetics 44, 821–824 (2012).

[100] B. Han, E. Eskin, Interpreting Meta-Analyses of Genome-Wide Association Studies. PLoS Genetics 8, e1002555–11 (2012).

[101] H. Ongen, et al., Estimating the causal tissues for complex traits and diseases. Nature Genetics 49, 1676–1683 (2017).

[102] A. Majumdar, et al., Leveraging eQTLs to identify individual-level tissue of interest for a complex trait. bioRxiv (2019).

[103] Y.-F. Huang, B. Gulko, A. Siepel, Fast, scalable prediction of deleterious noncoding variants from functional and population genomic data. Nature Genetics 49, 618–624 (2017).

[104] J. R. Davis, et al., An Efficient Multiple-Testing Adjustment for eQTL Studies that Accounts for Linkage Disequilibrium between Variants. American Journal of Human Genetics 98, 216–224 (2016).

[105] W. J. Astle, et al., The Allelic Landscape of Human Blood Cell Trait Variation and Links to Common Complex Disease. Cell 167, 1415–1429.e19 (2016).

[106] J. Malone, et al., Modeling sample variables with an Experimental Factor Ontology. Bioinformatics 26, 1112–1118 (2010).

[107] S. Köhler, et al., The Human Phenotype Ontology project: linking molecular biology and disease through phenotype data. Nucleic Acids Research 42, D966–74 (2014).

Acknowledgements

We thank the donors and their families for their generous gifts of organ donation for transplantation, and tissue donations for the GTEx research project; the Genomics Platform at the Broad Institute for data generation; J. Struewing for his support and leadership of the GTEx project; M. Khan and C. Stolte for the illustrations in Figure 1; and R. Do, D. Jordan, and M. Verbanck for providing GWAS pleiotropy scores.

Funding

This work was supported by the Common Fund of the Office of the Director, U.S. National Institutes of Health, and by NCI, NHGRI, NHLBI, NIDA, NIMH, NIA, NIAID, and NINDS through NIH contracts HHSN261200800001E (Leidos Prime contract with NCI: A.M.S., D.E.T., N.V.R., J.A.M., L.S., M.E.B., L.Q., T.K., D.B., K.R., A.U.), 10XS170 (NDRI: W.F.L., J.A.T., G.K., A.M., S.S., R.H., G.Wa., M.J., M.Wa., L.E.B., C.J., J.W., B.R., M.Hu., K.M., L.A.S., H.M.G., M.Mo., L.K.B.), 10XS171 (Roswell Park Cancer Institute: B.A.F., M.T.M., E.K., B.M.G., K.D.R., J.B.), 10X172 (Science Care Inc.), 12ST1039 (IDOX), 10ST1035 (Van Andel Institute: S.D.J., D.C.R., D.R.V.), HHSN268201000029C (Broad Institute: F.A., G.G., K.G.A., A.V.S., X.Li., E.T., S.G., A.G., S.A., K.H.H., D.T.N., K.H., S.R.M., J.L.N.), 5U41HG009494 (F.A., G.G., K.G.A.), and through NIH grants R01 DA006227-17 (Univ. of Miami Brain Bank: D.C.M., D.A.D.), Supplement to University of Miami grant DA006227 (D.C.M., D.A.D.), R01 MH090941 (Univ. of Geneva), R01 MH090951 and R01 MH090937 (Univ. of Chicago), R01 MH090936 (Univ. of North Carolina–Chapel Hill), R01MH101814 (M.M-A., V.W., S.B.M., R.G., E.T.D., D.G-M., A.V.), U01HG007593 (S.B.M.), R01MH101822 (C.D.B.), U01HG007598 (M.O., B.E.S.), U01MH104393 (A.P.F.), extension H002371 to 5U41HG002371 (W.J.K) as well as other funding sources: R01MH106842 (T.L., P.M., E.F., P.J.H.), R01HL142028 (T.L., Si.Ka., P.J.H.), R01GM122924 (T.L., S.E.C.), R01MH107666 (H.K.I.), P30DK020595 (H.K.I.), UM1HG008901 (T.L.), R01GM124486 (T.L.), R01HG010067 (Y.Pa.), R01HG002585 (G.Wa., M.St.), Gordon and Betty Moore Foundation GBMF 4559 (G.Wa., M.St.), 1K99HG009916-01 (S.E.C.), R01HG006855 (Se.Ka., R.E.H.), BIO2015-70777-P, Ministerio de Economia y Competitividad and FEDER funds (M.M-A., V.W., R.G., D.G-M.), la Caixa Foundation ID 100010434 under agreement LCF/BQ/SO15/52260001 (D.G-M.), NIH CTSA grant UL1TR002550-01 (P.M.), Marie-Skłodowska Curie fellowship H2020 Grant 706636 (S.K-H.), R35HG010718 (E.R.G.), FPU15/03635, Ministerio de Educación, Cultura y Deporte (M.M-A.), R01MH109905, 1R01HG010480 (A.Ba.), Searle Scholar Program (A.Ba.), R01HG008150 (S.B.M.), 5T32HG000044-22, NHGRI Institutional Training Grant in Genome Science (N.R.G.), EU IMI program (UE7-DIRECT-115317-1) (E.T.D., A.V.), FNS funded project RNA1 (31003A_149984) (E.T.D., A.V.), DK110919 (F.H.), F32HG009987 (F.H.), Massachusetts Lions Eye Research Fund Grant (A.R.H.).

Author Contributions

See Supplementary Material.

Competing interests

F.A. is an inventor on a patent application related to TensorQTL; S.E.C. is a co-founder, chief technology officer and stock owner at Variant Bio; E.R.G. is on the Editorial Board of Circulation Research, and does consulting for the City of Hope / Beckman Research Institut; E.T.D. is chairman and member of the board of Hybridstat LTD.; B.E.E. is on the scientific advisory boards of Celsius Therapeutics and Freenome; G.G. receives research funds from IBM and Pharmacyclics, and is an inventor on patent applications related to MuTect, ABSOLUTE, MutSig, POLYSOLVER and TensorQTL; S.B.M. is on the scientific advisory board of Prime Genomics Inc.; D.G.M. is a co-founder with equity in Goldfinch Bio, and has received research support from AbbVie, Astellas, Biogen, BioMarin, Eisai, Merck, Pfizer, and Sanofi-Genzyme; H.K.I. has received speaker honoraria from GSK and AbbVie.; T.L. is a scientific advisory board member of Variant Bio with equity and Goldfinch Bio. P.F. is member of the scientific advisory boards of Fabric Genomics, Inc., and Eagle Genomes, Ltd. P.G.F. is a partner of Bioinf2Bio.

Data and Materials Availability

All GTEx protected data are available via dbGaP (accession phs000424.v8). Access to the raw sequence data is now provided through the AnVIL platform (https://gtexportal.org/home/protectedDataAccess). Public-access data, including QTL summary statistics and expression levels, are available on the GTEx Portal, as downloadable files and through multiple data visualizations and browsable tables (www.gtexportal.org), as well as in the UCSC and Ensembl browsers. All components of the single tissue *cis*-QTL pipeline are available at https://github.com/broadinstitute/gtex-pipeline (https://doi.org/10.5281/zenodo.3727189), and analysis scripts are available at https://github.com/broadinstitute/gtex-v8 (https://doi.org/10.5281/zenodo.3930961). Residual GTEx biospecimens have been banked, and are available as a resource for further studies (access can be requested on the GTEx Portal, at https://www.gtexportal.org/home/samplesPage).

Supplementary Content

Supplementary Material, including methods, figures S1-S52 and tables S1-S9
Supplementary Tables S10-S16

Figure Legends

Figure 1. Sample and data types in the GTEx v8 study. (A) Illustration of the 54 tissue types examined (including 11 distinct brain regions and 2 cell lines), with sample numbers from genotyped donors in parentheses and color coding indicated in the adjacent circles. Tissues with ≥70 samples were included in QTL analyses. (B) Illustration of the core data types used throughout the study. Gene expression and splicing were quantified from bulk RNA-seq of heterogenous tissue samples, and local and distal genetic effects (*cis*-QTLs and *trans*-QTLs, respectively) were quantified across individuals for each tissue.

Figure 2. QTL discovery. (**A**) The number of genes with a *cis*-eQTL (eGenes) or *cis*-sQTL (sGenes) per tissue, as a function of sample size. See Fig. 1A for the legend of tissue colors. (**B)** Allelic heterogeneity of *cis*-eQTLs depicted as proportion of eGenes with ≥1 independent *cis*-eQTLs (blue stacked bars; left y-axis) and as a mean number of *cis*-eQTLs per gene (red dots; right y-axis). The tissues are ordered by sample size. **(C)** The number of genes with a *trans*-eQTL as a function of the number of *cis*-eGenes. **(D)** Sex-biased *cis*-eQTL for *AURKA* in skeletal muscle, where rs2273535-T is associated with increased *AURKA* expression in males ($p = 9.02 \times 10^{-27}$) but not in females ($p = 0.75$). (**E**) Population-biased *cis*-eQTL for *SLC44A5* in esophagus mucosa (allelic fold change = -2.85 and -4.82 and in African Americans (AA) and European Americans (EA), respectively; permutation p-value = 1.2×10^{-3}).

Figure 3. Fine mapping of *cis*-eQTLs. (A) Number of eGenes per tissue with variants fine-mapped with >0.5 posterior probability of causality, using three methods. The overall number of eGenes with at least one fine-mapped eVariant increases with sample size for all methods. However, this increase is in part driven by better statistical power to detect small effect size *cis*-eQTLs (aFC or allelic fold change ≤1 in log2 scale; see also fig. S14) with larger sample sizes, and the proportion of well fine-mapped eGenes with small effect sizes increases more modestly with sample size (bottom vs. top panels), indicating that such *cis*-eQTLs are generally more difficult to fine-map. (**B)** Enrichment of variants among experimentally validated regulatory variants, shown for the *cis*-eVariant with the best p-value (top eVariant), and those with posterior probability of causality >0.8 according to each of the three methods individually or all of them (consensus). Error bars: 95% CI. **(C**) The *cis*-eQTL signal for *CBX8* is fine-mapped to a credible set of three variants (red and purple diamonds), of which rs9896202 (purple diamond) overlaps a large number of transcription factor binding sites in ENCODE ChIP-seq data and disrupts the binding motif of *EGR1*. **(D)** The potential role of EGR1 binding driving this *cis*-eQTL is further supported by correlation between *EGR1* expression and the *CBX8 cis*-eQTL effect size across tissues.

Figure 4. Functional mechanisms of genetic regulatory effects. QTL enrichment in functional annotations for (**A**) *cis*-eQTLs and *cis*-sQTLs and for (**B**) *trans*-eQTLs. *cis*-QTL enrichment is shown as mean ± s.d. across tissues; *trans*-eQTL enrichment as 95% C.I. **(C)** Enrichment of lead *trans*-e/sVariants that have been tested for in *cis*-QTL effects being significant also *cis*-e/sVariants in the same tissue. * denotes significant enrichment, $p < 10^{-21}$. (**D**) Proportion of *trans*-eQTLs that are significant *cis*-eQTLs or mediated by *cis*-eQTLs. **(E)** *Trans* associations of *cis*-mediating genes identified through colocalization (PP4 > 0.8 and nominal association with discovery trans-eVariant $p < 10^{-5}$). Top: associations for four Thyroid *cis*-eQTLs (indicated by gene names); bottom: *cis*-mediating genes with ≥5 colocalizing *trans*-

eQTLs.

Figure 5. Regulatory mechanisms of GWAS loci. (A) GWAS enrichment of *cis*-eQTLs, *cis*-sQTLs, and *trans*-eQTLs measured with different approaches: enrichment calculated from GWAS summary statistics of the most significant *cis*-QTL per eGene/sGene with QTLEnrich and LD Score regression with all significant *cis*-QTLs (S-LDSC all *cis*-QTLs), simple QTL overlap enrichment with all GWAS catalog variants, and LD Score regression with fine-mapped *cis*-QTLs in the 95% credible set (S-LDSC credible set) and using posterior probability of causality as a continuous annotation (S-LDSC causal posterior). Enrichment is shown as mean and 95% CI. **(B)** Number of GWAS loci linked to e/sGenes through colocalization (ENLOC) and association (PrediXcan), aggregated across tissues. (**C)** Concordance of mediated effects among independent *cis*-eQTLs for the same gene, shown for different levels of regional colocalization probability (RCP (*32*)), which is used as a proxy for the gene's causality. As the null, we show the concordance for LD matched genes without colocalization. (**D)** Proportion of colocalized *cis*-eQTLs with a matching phenotype for genes with different level of rare variant trait association in the UK Biobank (UKB). (**E)** Horizontal GWAS trait pleiotropy score distribution for *cis*-eQTLs that regulate multiple vs. a single gene (left), and for *cis*-eQTLs that are tissue-shared vs. specific.

Figure 6. Tissue-specificity of *cis*-QTLs. (**A)** Tissue clustering with pairwise Spearman correlation of *cis*-eQTL effect sizes. (**B)** Similarity of tissue clustering across core data types quantified using median pairwise Rand index calculated across tissues. (**C)** Tissue activity of *cis* expression and splicing QTLs, where an eQTL was considered active in a tissue if it had a *mashr* local false sign rate (LFSR, equivalent to FDR) of < 5%. This is shown for all *cis*-QTLs and only those that could be tested in all 49 tissues (red and blue). **(D)** Spearman correlation (corr.) between *cis*-eQTL effect size and eGene expression level across tissues. *cis*-eQTL counts are shown for those not tested due to low expression level, tested but without significant (FDR < 5%) correlation (uncorrelated), a significant correlation but effect sizes crossed zero which made the correlation direction unclear (uninterpretable), positively correlated, and negatively correlated. (**E-F)** The effect of genomic function on *cis*-QTL tissue sharing modeled using logistic regression with functional annotations (**E**) and chromatin state (**F**). CTCF Peak, Motif, TF Peak, and DHS indicate if the *cis*-QTL lies in a region annotated as having one of these features in any of the Ensembl Regulatory Build tissues. For chromatin states, model coefficients are shown for the discovery and replication tissues that have the same or different chromatin states.

Figure 7. Cell type interacting *cis*-eQTLs and *cis*-sQTLs. (A) Number of cell type interacting *cis*-eQTLs and *cis*-sQTLs (ieQTLs and isQTLs, respectively) discovered in seven tissue-cell type pairs, with shading indicating whether the ieGene or isGene was discovered by *cis*-eQTL/*cis*-sQTL analysis in bulk tissue. Colored dots are proportional to sample size. (**B**) Functional enrichment of neutrophil ieQTLs and isQTLs compared to *cis*-eQTLs and *cis*-sQTLs from whole blood. (**C**) Proportion of conditionally independent *cis*-eQTLs per eGene, for eGenes that do or do not have ieQTLs in GTEx, and for eGenes that have shared (= eQTLs) or non-shared (≠ eQTLs) *cis*-eQTL across five sorted blood cell types. (**D**) Whole blood *cis*-eQTL p-value landscape for *NCOA4*, for the standard analysis (top row, Unconditional) and for two independent *cis*-eQTLs (bottom rows). In a data set of 5 sorted cell types (*56*), analyses of all cell types yielded a lead eVariant, rs2926494 (left), which is in high LD with the first independent *cis*-eQTL but not the second. The lead variant in monocyte *cis*-eQTL analysis, rs10740051, is in high LD with the second conditional *cis*-eQTL, indicating that this *cis*-eQTL is active specifically in monocytes. Thus, the full GTEx whole blood *cis*-eQTL pattern and allelic heterogeneity is composed of *cis*-eQTLs that are active in different cell types.

(E) COLOC posterior probability (PP4) of GWAS colocalization with whole blood ieQTLs and eQTLs of the same eGene. 349 gene-trait combinations across 132 genes and 36 GWAS traits showed evidence of colocalization (PP4 > 0.5) with an ieQTL and/or eQTL.

Authors

First author
* Alphabetical order

Lead Analysts*
François Aguet[1#], Alvaro N Barbeira[2], Rodrigo Bonazzola[2], Andrew Brown[3,4], Stephane E Castel[5,6], Brian Jo[7,8], Silva Kasela[5,6], Sarah Kim-Hellmuth[5,6,9], Yanyu Liang[2], Meritxell Oliva[2,10], Princy Parsana[11]

Analysts*
Elise D Flynn[5,6], Laure Fresard[12], Eric R Gamazon[13,14,15,16], Andrew R Hamel[17,1], Yuan He[18], Farhad Hormozdiari[19,1], Pejman Mohammadi[5,6,20,21], Manuel Muñoz-Aguirre[22,23], YoSon Park[24,25], Ashis Saha[11], Ayellet V Segrè[1,17], Benjamin J Strober[18], Xiaoquan Wen[26], Valentin Wucher[22]

Manuscript Working Group*
François Aguet[1], Kristin G Ardlie[1], Alvaro N Barbeira[2], Alexis Battle[18,11], Rodrigo Bonazzola[2], Andrew Brown[3,4], Christopher D Brown[24], Stephane E Castel[5,6], Nancy Cox[16], Sayantan Das[26], Emmanouil T Dermitzakis[3,27,28], Barbara E Engelhardt[7,8], Elise D Flynn[5,6], Laure Fresard[12], Eric R Gamazon[13,14,15,16], Diego Garrido-Martín[22], Nicole R Gay[29], Gad Getz[1,30], Roderic Guigó[22,31], Andrew R Hamel[17,1], Robert E Handsaker[32,33,34], Yuan He[18], Paul J Hoffman[5], Farhad Hormozdiari[19,1], Hae Kyung Im[2], Brian Jo[7,8], Silva Kasela[5,6], Seva Kashin[32,33,34], Sarah Kim-Hellmuth[5,6,9], Alan Kwong[26], Tuuli Lappalainen[5,6], Xiao Li[1], Yanyu Liang[2], Daniel G MacArthur[33,35], Pejman Mohammadi[5,6,20,21], Stephen B Montgomery[12,29], Manuel Muñoz-Aguirre[22,23], Meritxell Oliva[2,10], YoSon Park[24,25], Princy Parsana[11], John M Rouhana[17,1], Ashis Saha[11], Ayellet V Segrè[1,17], Matthew Stephens[36], Barbara E Stranger[2,37], Benjamin J Strober[18], Ellen Todres[1], Ana Viñuela[38,3,27,28], Gao Wang[36], Xiaoquan Wen[26], Valentin Wucher[22], Yuxin Zou[39]

Analysis Team Leaders*
François Aguet[1], Alexis Battle[18,11], Andrew Brown[3,4], Stephane E Castel[5,6], Barbara E Engelhardt[7,8], Farhad Hormozdiari[19,1], Hae Kyung Im[2], Sarah Kim-Hellmuth[5,6,9], Meritxell Oliva[2,10], Barbara E Stranger[2,37], Xiaoquan Wen[26]

Senior Leadership*
Kristin G Ardlie[1], Alexis Battle[18,11], Christopher D Brown[24], Nancy Cox[16], Emmanouil T Dermitzakis[3,27,28], Barbara E Engelhardt[7,8], Gad Getz[1,30], Roderic Guigó[22,31], Hae Kyung Im[2], Tuuli Lappalainen[5,6], Stephen B Montgomery[12,29], Barbara E Stranger[2,37]

Manuscript Writing Group
François Aguet[1], Hae Kyung Im[2], Alexis Battle[18,11], Kristin G Ardlie[1], Tuuli Lappalainen[5,6]

Corresponding Authors

François Aguet[1], Kristin G Ardlie[1], Tuuli Lappalainen[5,6]

GTEx Consortium*

Laboratory and Data Analysis Coordinating Center (LDACC): François Aguet[1], Shankara Anand[1], Kristin G Ardlie[1], Stacey Gabriel[1], Gad Getz[1,30], Aaron Graubert[1], Kane Hadley[1], Robert E Handsaker[32,33,34], Katherine H Huang[1], Seva Kashin[32,33,34], Xiao Li[1], Daniel G MacArthur[33,35], Samuel R Meier[1], Jared L Nedzel[1], Duyen T Nguyen[1], Ayellet V Segrè[1,17], Ellen Todres[1]

Analysis Working Group (funded by GTEx project grants):

François Aguet[1], Shankara Anand[1], Kristin G Ardlie[1], Brunilda Balliu[40], Alvaro N Barbeira[2], Alexis Battle[18,11], Rodrigo Bonazzola[2], Andrew Brown[3,4], Christopher D Brown[24], Stephane E Castel[5,6], Don Conrad[41,42], Daniel J Cotter[29], Nancy Cox[16], Sayantan Das[26], Olivia M de Goede[29], Emmanouil T Dermitzakis[3,27,28], Jonah Einson[43,5], Barbara E Engelhardt[7,8], Eleazar Eskin[44], Tiffany Y Eulalio[45], Nicole M Ferraro[45], Elise D Flynn[5,6], Laure Fresard[12], Eric R Gamazon[13,14,15,16], Diego Garrido-Martín[22], Nicole R Gay[29], Gad Getz[1,30], Michael J Gloudemans[45], Aaron Graubert[1], Roderic Guigó[22,31], Kane Hadley[1], Andrew R Hamel[17,1], Robert E Handsaker[32,33,34], Yuan He[18], Paul J Hoffman[5], Farhad Hormozdiari[19,1], Lei Hou[46,1], Katherine H Huang[1], Hae Kyung Im[2], Brian Jo[7,8], Silva Kasela[5,6], Seva Kashin[32,33,34], Manolis Kellis[46,1], Sarah Kim-Hellmuth[5,6,9], Alan Kwong[26], Tuuli Lappalainen[5,6], Xiao Li[1], Xin Li[12], Yanyu Liang[2], Daniel G MacArthur[33,35], Serghei Mangul[44,47], Samuel R Meier[1], Pejman Mohammadi[5,6,20,21], Stephen B Montgomery[12,29], Manuel Muñoz-Aguirre[22,23], Daniel C Nachun[12], Jared L Nedzel[1], Duyen T Nguyen[1], Andrew B Nobel[48], Meritxell Oliva[2,10], YoSon Park[24,25], Yongjin Park[46,1], Princy Parsana[11], Abhiram S Rao[49], Ferran Reverter[50], John M Rouhana[17,1], Chiara Sabatti[51], Ashis Saha[11], Ayellet V Segrè[1,17], Andrew D Skol[2,52], Matthew Stephens[36], Barbara E Stranger[2,37], Benjamin J Strober[18], Nicole A Teran[12], Ellen Todres[1], Ana Viñuela[38,3,27,28], Gao Wang[36], Xiaoquan Wen[26], Fred Wright[53], Valentin Wucher[22], Yuxin Zou[39]

Analysis Working Group (not funded by GTEx project grants): Pedro G Ferreira[54,55,56,57], Gen Li[58], Marta Melé[59], Esti Yeger-Lotem[60,61]

Leidos Biomedical - Project Management: Mary E Barcus[62], Debra Bradbury[62], Tanya Krubit[62], Jeffrey A McLean[62], Liqun Qi[62], Karna Robinson[62], Nancy V Roche[62], Anna M Smith[62], Leslie Sobin[62], David E Tabor[62], Anita Undale[62]

Biospecimen collection source sites: Jason Bridge[63], Lori E Brigham[64], Barbara A Foster[65], Bryan M Gillard[65], Richard Hasz[66], Marcus Hunter[67], Christopher Johns[68], Mark Johnson[69], Ellen Karasik[65], Gene Kopen[70], William F Leinweber[70], Alisa McDonald[70], Michael T Moser[65], Kevin Myer[67], Kimberley D Ramsey[65], Brian Roe[67], Saboor Shad[70], Jeffrey A Thomas[70,69], Gary Walters[69], Michael Washington[69], Joseph Wheeler[68]

Biospecimen core resource: Scott D Jewell[71], Daniel C Rohrer[71], Dana R Valley[71]

Brain bank repository: David A Davis[72], Deborah C Mash[72]

Pathology: Mary E Barcus[62], Philip A Branton[73], Leslie Sobin[62]

ELSI study: Laura K Barker[74], Heather M Gardiner[74], Maghboeba Mosavel[75], Laura A Siminoff[74]

Genome Browser Data Integration & Visualization: Paul Flicek[76], Maximilian Haeussler[77], Thomas Juettemann[76], W James Kent[77], Christopher M Lee[77], Conner C Powell[77], Kate R Rosenbloom[77], Magali Ruffier[76], Dan Sheppard[76], Kieron Taylor[76], Stephen J Trevanion[76], Daniel R Zerbino[76]

eGTEx groups: Nathan S Abell[29], Joshua Akey[78], Lin Chen[10], Kathryn Demanelis[10], Jennifer A Doherty[79], Andrew P Feinberg[80], Kasper D Hansen[81], Peter F Hickey[82], Lei Hou[46,1], Farzana Jasmine[10], Lihua Jiang[29], Rajinder Kaul[83,84], Manolis Kellis[46,1], Muhammad G Kibriya[10], Jin Billy Li[29], Qin Li[29], Shin Lin[85], Sandra E Linder[29], Stephen B Montgomery[12,29], Meritxell Oliva[2,10], Yongjin Park[46,1], Brandon L Pierce[10], Lindsay F Rizzardi[86], Andrew D Skol[2,52], Kevin S Smith[12], Michael Snyder[29], John Stamatoyannopoulos[83,87], Barbara E Stranger[2,37], Hua Tang[29], Meng Wang[29]

NIH program management: Philip A Branton[73], Latarsha J Carithers[73,88], Ping Guan[73], Susan E Koester[89], A. Roger Little[90], Helen M Moore[73], Concepcion R Nierras[91], Abhi K Rao[73], Jimmie B Vaught[73], Simona Volpi[92]

Affiliations

1. The Broad Institute of MIT and Harvard, Cambridge, MA, USA
2. Section of Genetic Medicine, Department of Medicine, The University of Chicago, Chicago, IL, USA
3. Department of Genetic Medicine and Development, University of Geneva Medical School, Geneva, Switzerland
4. Population Health and Genomics, University of Dundee, Dundee, Scotland, UK
5. New York Genome Center, New York, NY, USA
6. Department of Systems Biology, Columbia University, New York, NY, USA
7. Department of Computer Science, Princeton University, Princeton, NJ, USA
8. Center for Statistics and Machine Learning, Princeton University, Princeton, NJ, USA
9. Statistical Genetics, Max Planck Institute of Psychiatry, Munich, Germany
10. Department of Public Health Sciences, The University of Chicago, Chicago, IL, USA
11. Department of Computer Science, Johns Hopkins University, Baltimore, MD, USA
12. Department of Pathology, Stanford University, Stanford, CA, USA
13. Data Science Institute, Vanderbilt University, Nashville, TN, USA
14. Clare Hall, University of Cambridge, Cambridge, UK
15. MRC Epidemiology Unit, University of Cambridge, Cambridge, UK
16. Division of Genetic Medicine, Department of Medicine, Vanderbilt University Medical Center, Nashville, TN, USA
17. Ocular Genomics Institute, Massachusetts Eye and Ear, Harvard Medical School, Boston, MA, USA
18. Department of Biomedical Engineering, Johns Hopkins University, Baltimore, MD, USA
19. Department of Epidemiology, Harvard T.H. Chan School of Public Health, Boston, MA, USA
20. Scripps Research Translational Institute, La Jolla, CA, USA
21. Department of Integrative Structural and Computational Biology, The Scripps Research Institute, La Jolla, CA, USA
22. Centre for Genomic Regulation (CRG), The Barcelona Institute for Science and Technology, Barcelona, Catalonia, Spain
23. Department of Statistics and Operations Research, Universitat Polit√®cnica de Catalunya (UPC), Barcelona, Catalonia, Spain
24. Department of Genetics, University of Pennsylvania, Perelman School of Medicine, Philadelphia, PA, USA
25. Department of Systems Pharmacology and Translational Therapeutics, University of Pennsylvania, Perelman School of Medicine, Philadelphia, PA, USA
26. Department of Biostatistics, University of Michigan, Ann Arbor, MI, USA
27. Institute for Genetics and Genomics in Geneva (iGE3), University of Geneva, Geneva, Switzerland
28. Swiss Institute of Bioinformatics, Geneva, Switzerland
29. Department of Genetics, Stanford University, Stanford, CA, USA
30. Cancer Center and Department of Pathology, Massachusetts General Hospital, Boston, MA, USA
31. Universitat Pompeu Fabra (UPF), Barcelona, Catalonia, Spain
32. Department of Genetics, Harvard Medical School, Boston, MA, USA
33. Program in Medical and Population Genetics, The Broad Institute of Massachusetts Institute of Technology and Harvard University, Cambridge, MA, USA
34. Stanley Center for Psychiatric Research, Broad Institute, Cambridge, MA, USA
35. Analytic and Translational Genetics Unit, Massachusetts General Hospital, Boston, MA, USA
36. Department of Human Genetics, University of Chicago, Chicago, IL, USA
37. Center for Genetic Medicine, Department of Pharmacology, Northwestern University, Feinberg School of Medicine, Chicago, IL, USA
38. Department of Twin Research and Genetic Epidemiology, King‚Äôs College London, London, UK
39. Department of Statistics, University of Chicago, Chicago, IL, USA
40. Department of Biomathematics, University of California, Los Angeles, Los Angeles, CA, USA
41. Department of Genetics, Washington University School of Medicine, St. Louis, Missouri, USA

42. Department of Pathology & Immunology, Washington University School of Medicine, St. Louis, Missouri, USA
43. Department of Biomedical Informatics, Columbia University, New York, NY, USA
44. Department of Computer Science, University of California, Los Angeles, Los Angeles, CA, USA
45. Program in Biomedical Informatics, Stanford University School of Medicine, Stanford, CA, USA
46. Computer Science and Artificial Intelligence Laboratory, Massachusetts Institute of Technology, Cambridge, MA, USA
47. Department of Clinical Pharmacy, School of Pharmacy, University of Southern California, Los Angeles, CA, USA
48. Department of Statistics and Operations Research and Department of Biostatistics, University of North Carolina, Chapel Hill, NC, USA
49. Department of Bioengineering, Stanford University, Stanford, CA, USA
50. Department of Genetics, Microbiology and Statistics, University of Barcelona, Barcelona. Spain.
51. Departments of Biomedical Data Science and Statistics, Stanford University, Stanford, CA, USA
52. Department of Pathology and Laboratory Medicine, Ann & Robert H. Lurie Children's Hospital of Chicago, Chicago, IL, USA
53. Bioinformatics Research Center and Departments of Statistics and Biological Sciences, North Carolina State University, Raleigh, NC, USA
54. Department of Computer Sciences, Faculty of Sciences, University of Porto, Porto, Portugal
55. Instituto de InvestigacÃßaÃÉo e InovacÃßaÃÉo em SauÃÅde, University of Porto, Porto, Portugal
56. Institute of Molecular Pathology and Immunology, University of Porto, Porto, Portugal
57. Laboratory of Artificial Intelligence and Decision Support, Institute for Systems and Computer Engineering, Technology and Science, Porto, Portugal
58. Columbia University Mailman School of Public Health, New York, NY, USA
59. Life Sciences Department, Barcelona Supercomputing Center, Barcelona, Spain
60. Department of Clinical Biochemistry and Pharmacology, Ben-Gurion University of the Negev, Beer-Sheva, Israel
61. National Institute for Biotechnology in the Negev, Beer-Sheva, Israel
62. Leidos Biomedical, Rockville, MD, USA
63. UNYTS, Buffalo, NY, USA
64. Washington Regional Transplant Community, Annandale, VA, USA
65. Therapeutics, Roswell Park Comprehensive Cancer Center, Buffalo, NY, USA
66. Gift of Life Donor Program, Philadelphia, PA, USA
67. LifeGift, Houston, TX, USA
68. Center for Organ Recovery and Education, Pittsburgh, PA, USA
69. LifeNet Health, Virginia Beach, VA. USA
70. National Disease Research Interchange, Philadelphia, PA, USA
71. Van Andel Research Institute, Grand Rapids, MI, USA
72. Department of Neurology, University of Miami Miller School of Medicine, Miami, FL, USA
73. Biorepositories and Biospecimen Research Branch, Division of Cancer Treatment and Diagnosis, National Cancer Institute, Bethesda, MD, USA
74. Temple University, Philadelphia, PA, USA
75. Virgina Commonwealth University, Richmond, VA, USA
76. European Molecular Biology Laboratory, European Bioinformatics Institute, Hinxton, United Kingdom
77. Genomics Institute, University of California, Santa Cruz, Santa Cruz, CA, USA
78. Carl Icahn Laboratory, Princeton University, Princeton, NJ, USA
79. Department of Population Health Sciences, The University of Utah, Salt Lake City, Utah, USA
80. Departments of Medicine, Biomedical Engineering, and Mental Health, Johns Hopkins University, Baltimore, MD, USA
81. Department of Biostatistics, Bloomberg School of Public Health, Johns Hopkins University, Baltimore, MD, USA
82. Department of Medical Biology, The Walter and Eliza Hall Institute of Medical Research, Parkville, Victoria, Australia
83. Altius Institute for Biomedical Sciences, Seattle, WA, USA
84. Division of Genetics, University of Washington, Seattle, WA, University of Washington, Seattle, WA, USA
85. Department of Cardiology, University of Washington, Seattle, WA, USA
86. HudsonAlpha Institute for Biotechnology, Huntsville, AL, USA
87. Genome Sciences, University of Washington, Seattle, WA, USA

88. National Institute of Dental and Craniofacial Research, Bethesda, MD, USA
89. Division of Neuroscience and Basic Behavioral Science, National Institute of Mental Health, National Institutes of Health, Bethesda, MD, USA
90. National Institute on Drug Abuse, Bethesda, MD, USA
91. Office of Strategic Coordination, Division of Program Coordination, Planning and Strategic Initiatives, Office of the Director, National Institutes of Health, Rockville, MD, USA
92. Division of Genomic Medicine, National Human Genome Research Institute, Bethesda, MD, USA

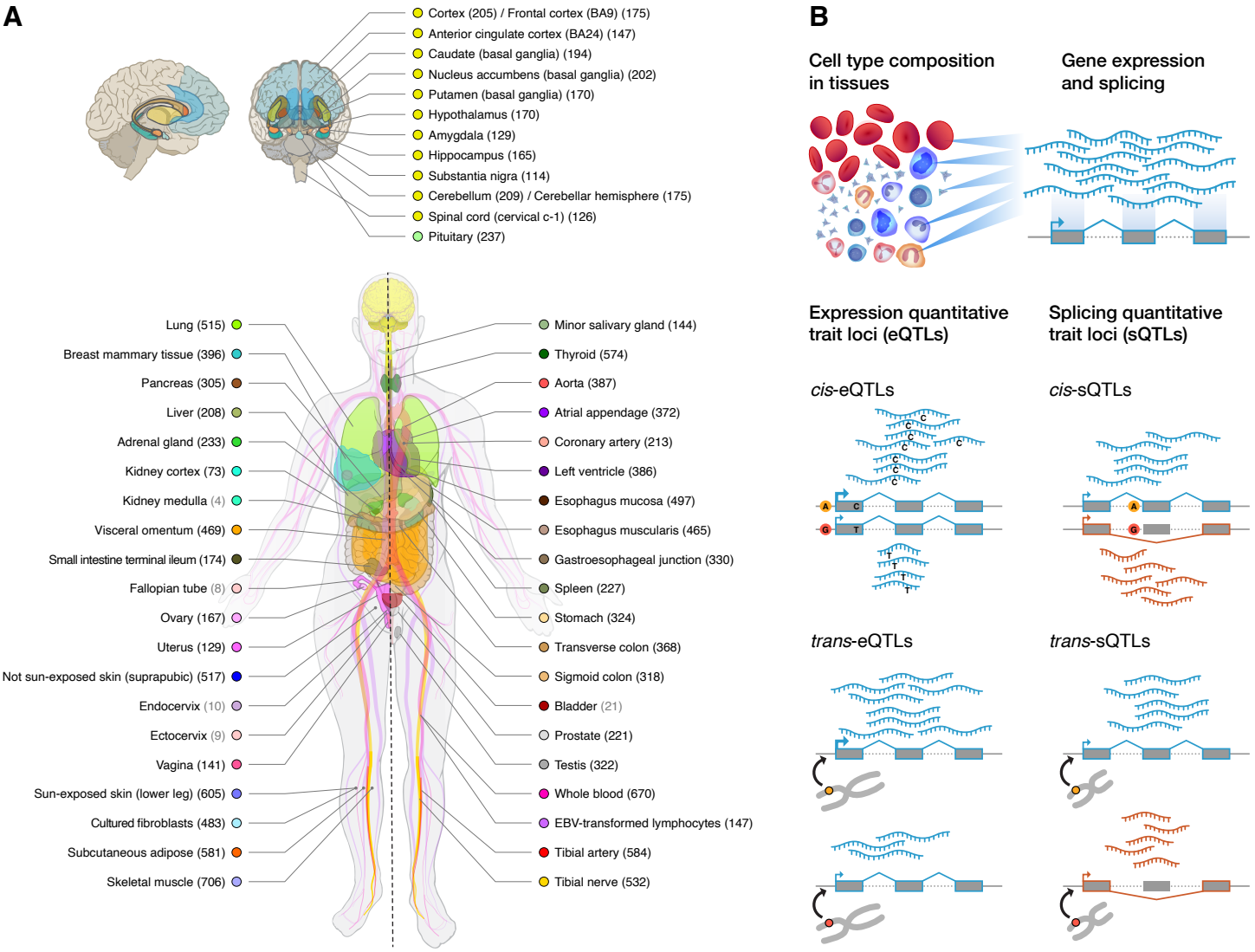
A
Cortex (205) / Frontal cortex (BA9) (175)
Anterior cingulate cortex (BA24) (147)
Caudate (basal ganglia) (194)
Nucleus accumbens (basal ganglia) (202)
Putamen (basal ganglia) (170)
Hypothalamus (170)
Amygdala (129)
Hippocampus (165)
Substantia nigra (114)
Cerebellum (209) / Cerebellar hemisphere (175)
Spinal cord (cervical c-1) (126)
Pituitary (237)
Lung (515)
Breast mammary tissue (396)
Pancreas (305)
Liver (208)
Adrenal gland (233)
Kidney cortex (73)
Kidney medulla (4)
Visceral omentum (469)
Small intestine terminal ileum (174)
Fallopian tube (8)
Ovary (167)
Uterus (129)
Not sun-exposed skin (suprapubic) (517)
Endocervix (10)
Ectocervix (9)
Vagina (141)
Sun-exposed skin (lower leg) (605)
Cultured fibroblasts (483)
Subcutaneous adipose (581)
Skeletal muscle (706)
Minor salivary gland (144)
Thyroid (574)
Aorta (387)
Atrial appendage (372)
Coronary artery (213)
Left ventricle (386)
Esophagus mucosa (497)
Esophagus muscularis (465)
Gastroesophageal junction (330)
Spleen (227)
Stomach (324)
Transverse colon (368)
Sigmoid colon (318)
Bladder (21)
Prostate (221)
Testis (322)
Whole blood (670)
EBV-transformed lymphocytes (147)
Tibial artery (584)
Tibial nerve (532)
B
Cell type composition in tissues
Gene expression and splicing
Expression quantitative trait loci (eQTLs)
Splicing quantitative trait loci (sQTLs)
cis-eQTLs
cis-sQTLs
trans-eQTLs
trans-sQTLs

Figure 1

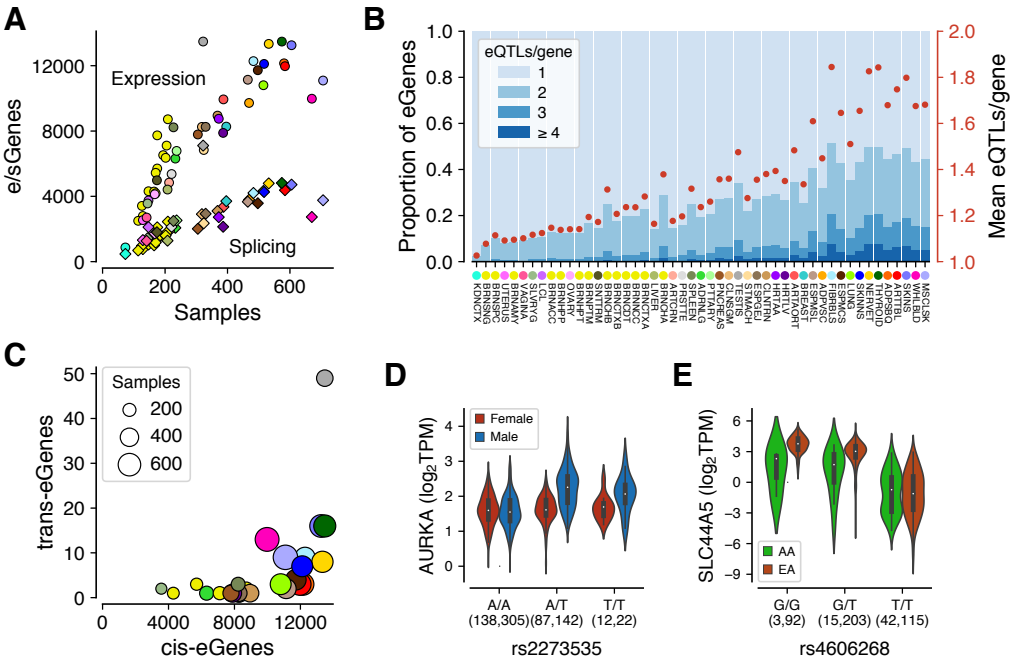
A
e/sGenes
Expression
Splicing
Samples
B
Proportion of eGenes
Mean eQTLs/gene
eQTLs/gene
1
2
3
≥ 4
C
trans-eGenes
cis-eGenes
Samples
200
400
600
D
AURKA (log2TPM)
Female
Male
A/A (138,305)
A/T (87,142)
T/T (12,22)
rs2273535
E
SLC44A5 (log2TPM)
AA
EA
G/G (3,92)
G/T (15,203)
T/T (42,115)
rs4606268

Figure 2

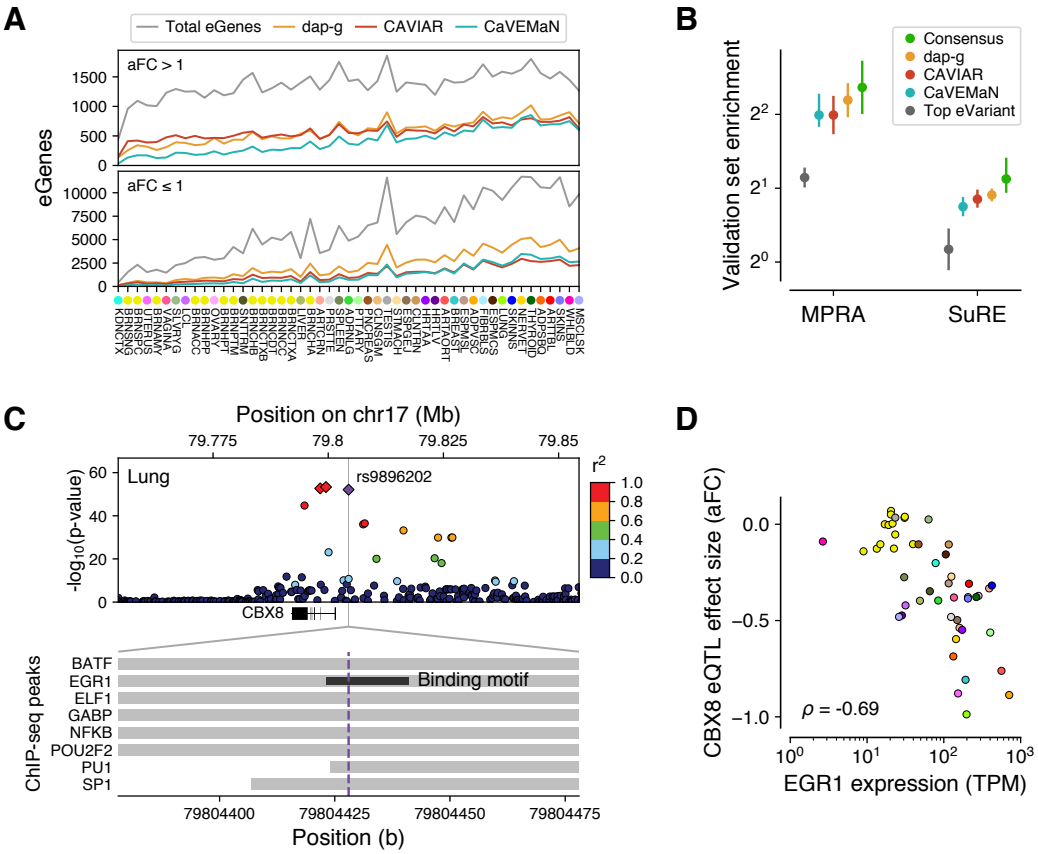
A
Total eGenes
dap-g
CAVIAR
CaVEMaN
aFC > 1
aFC ≤ 1
eGenes
B
Consensus
dap-g
CAVIAR
CaVEMaN
Top eVariant
Validation set enrichment
MPRA
SuRE
C
Position on chr17 (Mb)
Lung
rs9896202
-log10(p-value)
r2
CBX8
ChIP-seq peaks
BATF
EGR1
ELF1
GABP
NFKB
POU2F2
PU1
SP1
Binding motif
Position (b)
D
CBX8 eQTL effect size (aFC)
ρ = -0.69
EGR1 expression (TPM)

Figure 3

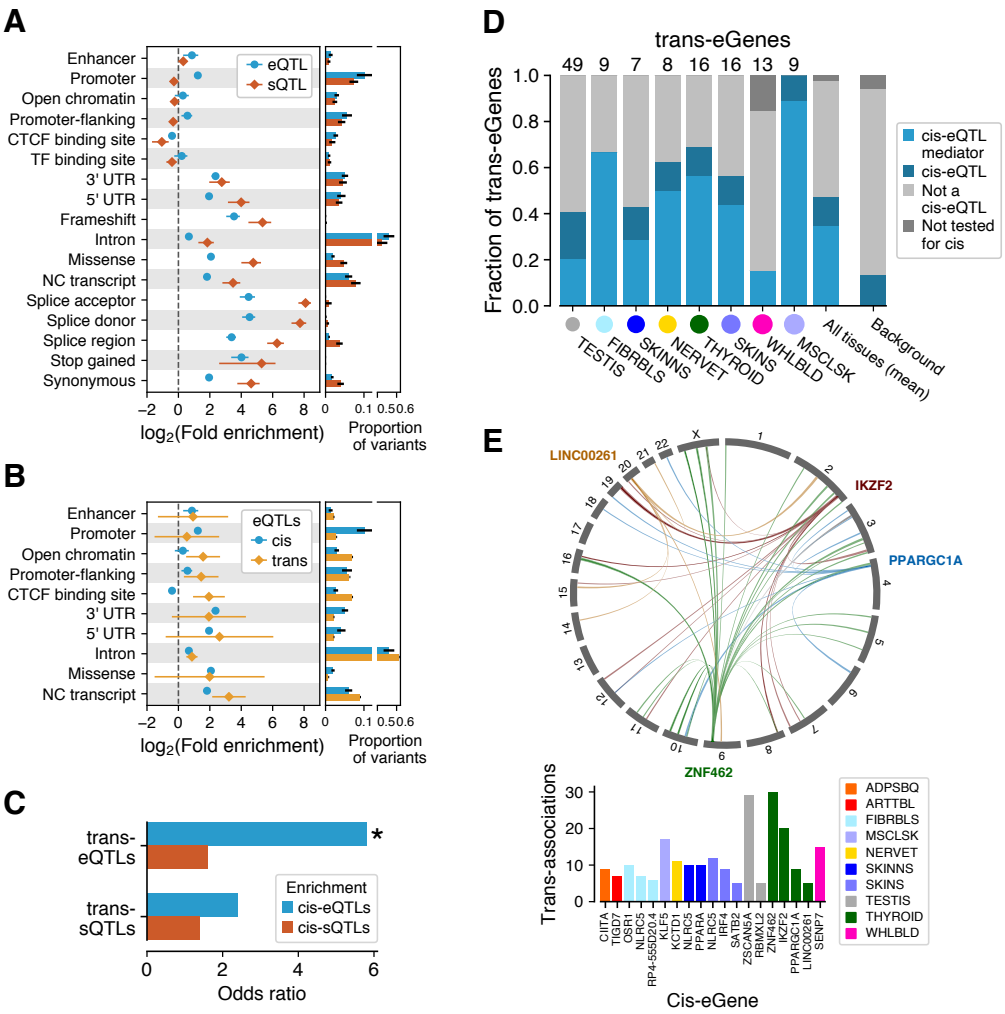
A
Enhancer
Promoter
Open chromatin
Promoter-flanking
CTCF binding site
TF binding site
3' UTR
5' UTR
Frameshift
Intron
Missense
NC transcript
Splice acceptor
Splice donor
Splice region
Stop gained
Synonymous
eQTL
sQTL
log2(Fold enrichment)
Proportion of variants
B
eQTLs
cis
trans
C
trans-eQTLs
trans-sQTLs
Enrichment
cis-eQTLs
cis-sQTLs
Odds ratio
D
trans-eGenes
Fraction of trans-eGenes
cis-eQTL mediator
cis-eQTL
Not a cis-eQTL
Not tested for cis
TESTIS
FIBRBLS
SKINNS
NERVET
THYROID
SKINS
WHLBLD
MSCLSK
All tissues (mean)
Background
E
LINC00261
IKZF2
PPARGC1A
ZNF462
Trans-associations
Cis-eGene
ADPSBQ
ARTTBL
FIBRBLS
MSCLSK
NERVET
SKINNS
SKINS
TESTIS
THYROID
WHLBLD

Figure 4

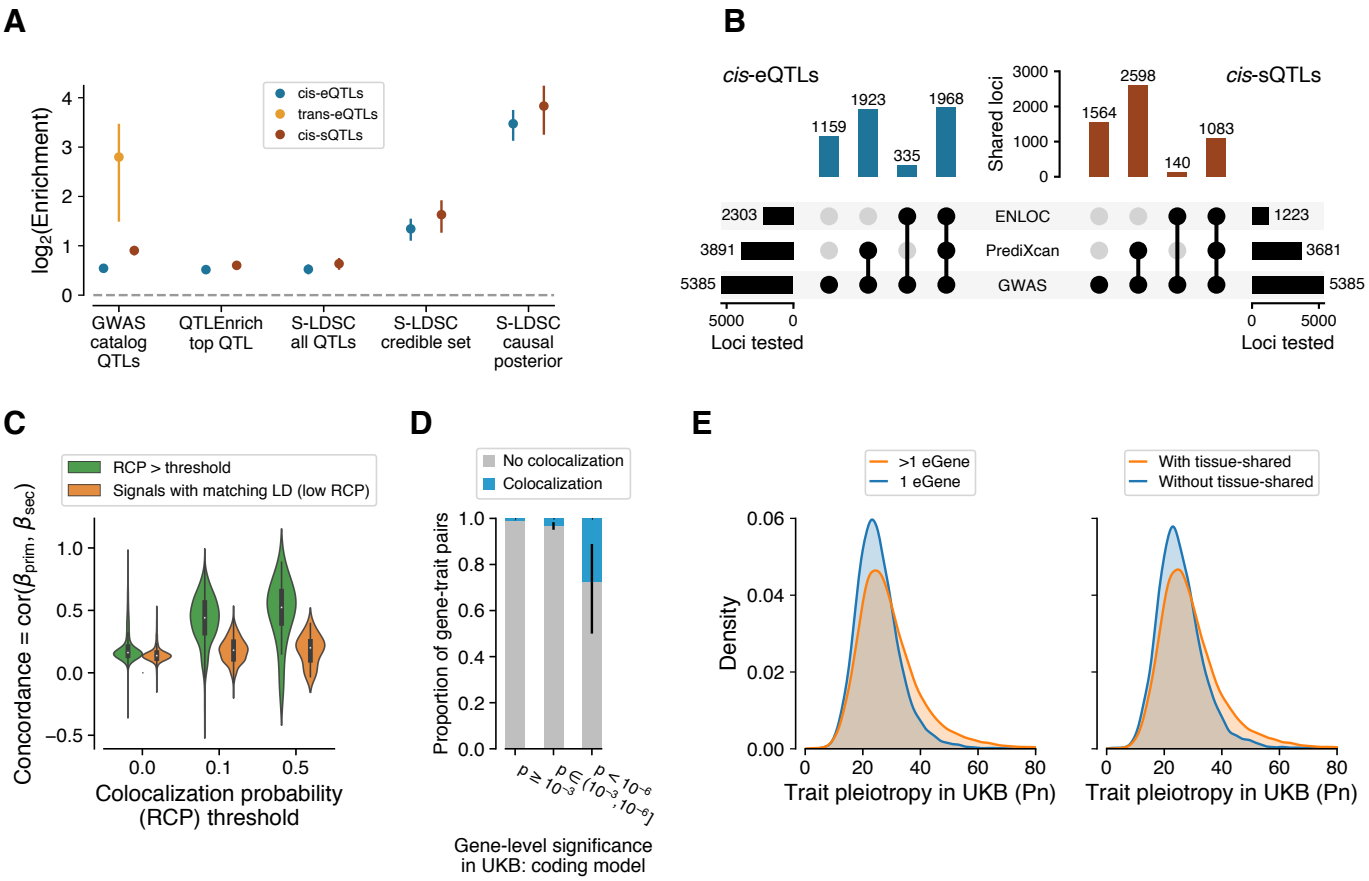
A
cis-eQTLs
trans-eQTLs
cis-sQTLs
log2(Enrichment)
GWAS catalog QTLs
QTLEnrich top QTL
S-LDSC all QTLs
S-LDSC credible set
S-LDSC causal posterior
B
cis-eQTLs
cis-sQTLs
Shared loci
1159
1923
1968
335
1564
2598
140
1083
2303
3891
5385
ENLOC
PrediXcan
GWAS
1223
3681
5385
Loci tested
Loci tested
C
RCP > threshold
Signals with matching LD (low RCP)
Concordance = cor(βprim, βsec)
Colocalization probability (RCP) threshold
D
No colocalization
Colocalization
Proportion of gene-trait pairs
Gene-level significance in UKB: coding model
E
>1 eGene
1 eGene
With tissue-shared
Without tissue-shared
Density
Trait pleiotropy in UKB (Pn)
Trait pleiotropy in UKB (Pn)

Figure 5

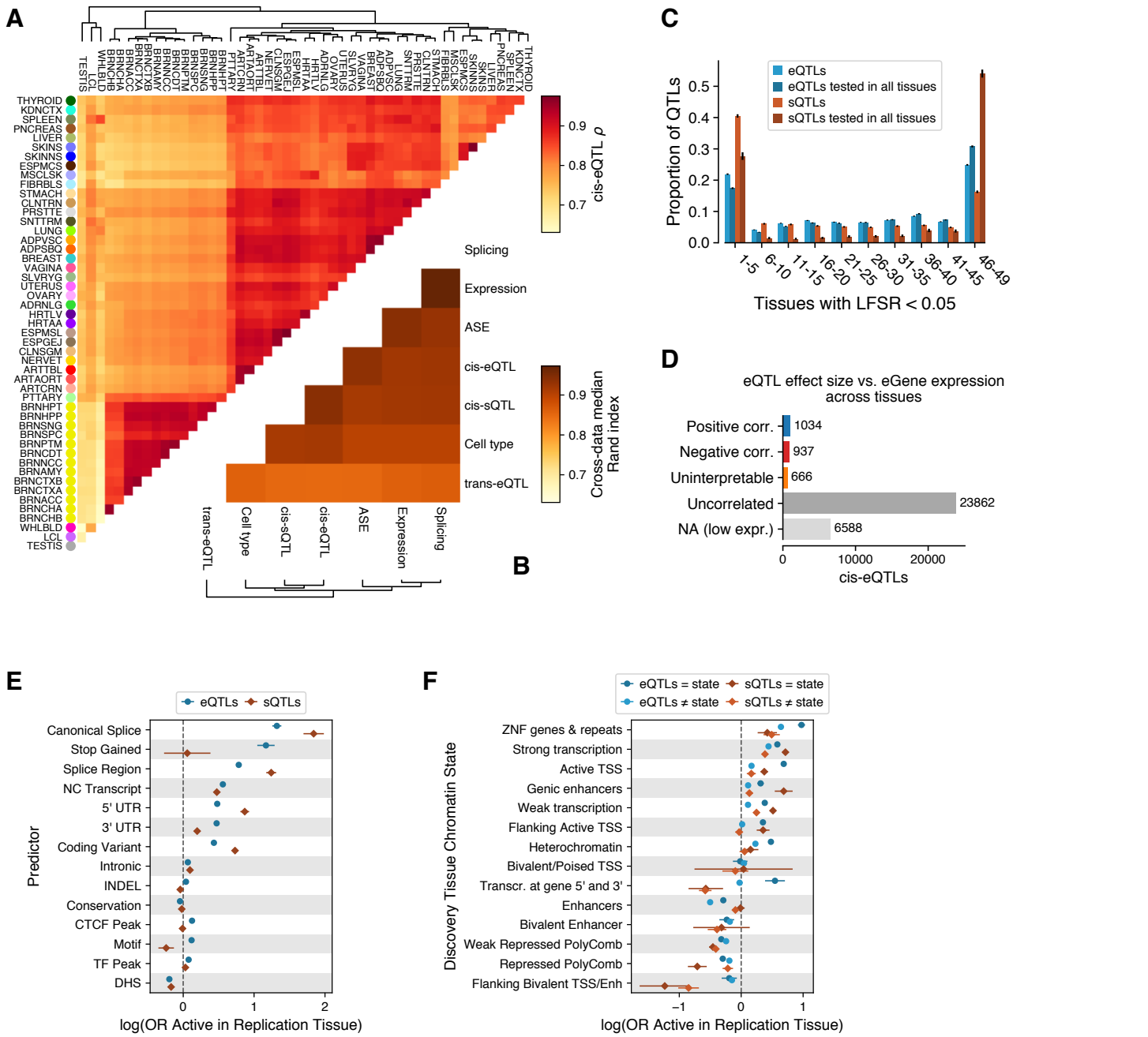
A
cis-eQTL ρ
Splicing
Expression
ASE
cis-eQTL
cis-sQTL
Cell type
trans-eQTL
Cross-data median Rand index
B
C
eQTLs
eQTLs tested in all tissues
sQTLs
sQTLs tested in all tissues
Proportion of QTLs
Tissues with LFSR < 0.05
D
eQTL effect size vs. eGene expression across tissues
Positive corr.
Negative corr.
Uninterpretable
Uncorrelated
NA (low expr.)
1034
937
666
23862
6588
cis-eQTLs
E
eQTLs
sQTLs
Predictor
Canonical Splice
Stop Gained
Splice Region
NC Transcript
5' UTR
3' UTR
Coding Variant
Intronic
INDEL
Conservation
CTCF Peak
Motif
TF Peak
DHS
log(OR Active in Replication Tissue)
F
eQTLs = state
sQTLs = state
eQTLs ≠ state
sQTLs ≠ state
Discovery Tissue Chromatin State
ZNF genes & repeats
Strong transcription
Active TSS
Genic enhancers
Weak transcription
Flanking Active TSS
Heterochromatin
Bivalent/Poised TSS
Transcr. at gene 5' and 3'
Enhancers
Bivalent Enhancer
Weak Repressed PolyComb
Repressed PolyComb
Flanking Bivalent TSS/Enh
log(OR Active in Replication Tissue)

Figure 6

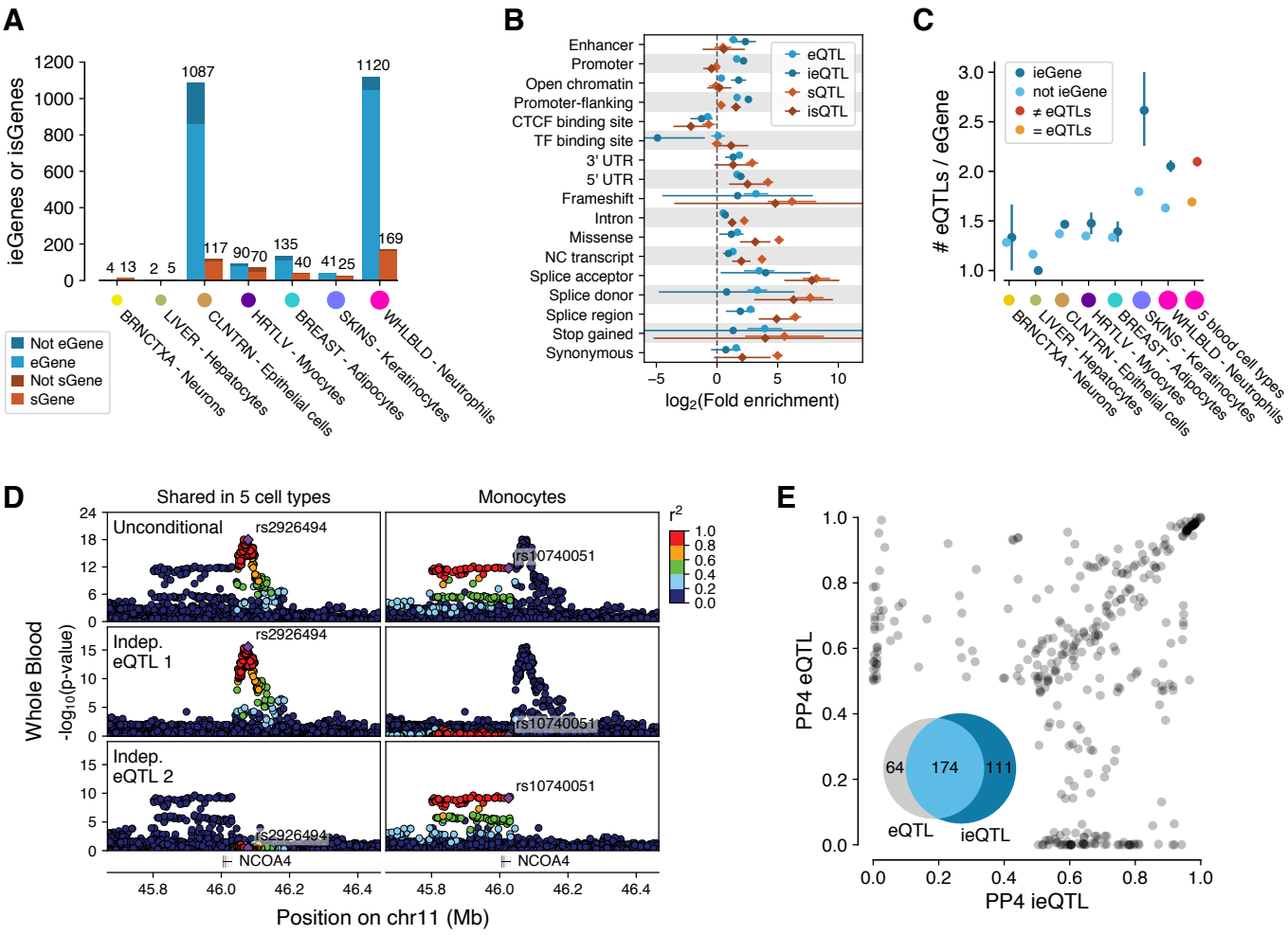
A
ieGenes or isGenes
1200
1000
800
600
400
200
0
4 13
2 5
1087
117
90 70
135
40
41 25
1120
169
Not eGene
eGene
Not sGene
sGene
BRNCTXA - Neurons
LIVER - Hepatocytes
CLNTRN - Epithelial cells
HRTLV - Myocytes
BREAST - Adipocytes
SKINS - Keratinocytes
WHLBLD - Neutrophils
B
Enhancer
Promoter
Open chromatin
Promoter-flanking
CTCF binding site
TF binding site
3' UTR
5' UTR
Frameshift
Intron
Missense
NC transcript
Splice acceptor
Splice donor
Splice region
Stop gained
Synonymous
eQTL
ieQTL
sQTL
isQTL
−5
0
5
10
log2(Fold enrichment)
C
eQTLs / eGene
3.0
2.5
2.0
1.5
1.0
ieGene
not ieGene
≠ eQTLs
= eQTLs
BRNCTXA - Neurons
LIVER - Hepatocytes
CLNTRN - Epithelial cells
HRTLV - Myocytes
BREAST - Adipocytes
SKINS - Keratinocytes
WHLBLD - Neutrophils
5 blood cell types
D
Shared in 5 cell types
Monocytes
Unconditional
rs2926494
rs10740051
Indep. eQTL 1
rs2926494
rs10740051
Indep. eQTL 2
rs10740051
rs2926494
NCOA4
NCOA4
Whole Blood
-log10(p-value)
r2
1.0
0.8
0.6
0.4
0.2
0.0
45.8
46.0
46.2
46.4
Position on chr11 (Mb)
E
PP4 eQTL
PP4 ieQTL
1.0
0.8
0.6
0.4
0.2
0.0
64
174
111
eQTL
ieQTL

Figure 7